Chemical Geology 529 (2019) 119240

Contents lists available at ScienceDirect

Chemical Geology

journal homepage: www.elsevier.com/locate/chemgeo

Combined boron, radiogenic (Nd, Pb, Sr), stable (C, O) isotopic and geochemical investigations of carbonatites from the Blue River Region, British Columbia (Canada): Implications for mantle sources and recycling of crustal carbon

Okay Çimen[a,b,*], Corinne Kuebler[a], Stefanie S. Simonetti[a], Loretta Corcoran[a], Roger Mitchell[c], Antonio Simonetti[a]

[a] University of Notre Dame, Department of Civil and Environmental Engineering and Earth Sciences, South Bend, IN 46556, USA
[b] Munzur University, Rare Earth Elements Application and Research Center, 62000 Tunceli, Turkey
[c] Department of Geology, Lakehead University, 955 Oliver Road, Thunder Bay, Ontario P7B 5E1, Canada

ARTICLE INFO

Editor: Catherine Chauvel

Keywords:
Boron isotopes
Mantle heterogeneity
Blue River carbonatites
Recycled crustal carbon
Collision-type tectonic environment

ABSTRACT

This study reports the combined major, minor and trace element compositions, and stable (C, O), radiogenic (Nd, Pb, and Sr) isotopic compositions, and first $\delta^{11}B$ isotopic data for the Fir, Felix, Gum, and Howard Creek carbonatites from the Blue River Region, British Columbia (Canada). These sill-like occurrences were intruded into Late Proterozoic strata during rifting and extensional episodes during the Late Cambrian and Devonian -Mississippian, and subsequently deformed and metamorphosed to amphibolite grade in relation to a collisional-type tectonic environment. The carbonatites at Fir, Gum, and Felix contain both calcite and dolomite, whereas the carbonatite at Howard Creek contains only calcite. The dolomite compositions reported here are consistent with those experimentally determined by direct partial melting of metasomatized peridotitic mantle. The combined major and trace element compositions and $\delta^{13}C_{PDB}$ (−5.37 to −4.85‰) and $\delta^{18}O_{SMOW}$ (9.14 to 9.62‰) values for all the samples investigated are consistent with those for primary igneous carbonate and support their mantle origin. However, these signatures cannot be attributed to closed system melt differentiation from a single parental melt. The initial Nd, Pb, and Sr isotopic ratios are highly variable and suggest generation from multiple, small degree parental melts derived from a heterogeneous mantle source. The $\delta^{11}B$ values for carbonates from Felix, Gum, and Howard Creek vary between −8.67 and −6.36‰, and overlap the range for asthenospheric mantle (−7.1 ± 0.9‰), whereas two samples from Fir yield heavier values of −3.98 and −2.47‰. The latter indicate the presence of recycled crustal carbon in their mantle source region, which is consistent with those for young (< 300 Ma) carbonatites worldwide. The radiogenic and B isotope results for the Blue River carbonatites are compared to those from contrasting, anorogenic tectonic settings at Chipman Lake, Fen, and Jacupiranga, and indicate that similar upper mantle sources are being tapped for carbonatite melt generation. The pristine, mantle-like $\delta^{11}B$ values reported here for the Blue River carbonatites clearly demonstrate that this isotope system is robust and was not perturbed by post-solidification tectono-metamorphic events. This observation indicates that B isotope signatures are a valuable tool for deciphering the nature of the upper mantle sources for carbonates of igneous origin.

1. Introduction

Carbonatites are unique igneous rocks with distinct compositional and mineralogical characteristics, which include high concentrations (i.e. 100's to 1000's of ppm) of Sr, Nd, REEs and volatiles (e.g., Bell and Simonetti, 2010; Jones et al., 2013), and consist > 50 vol% (silica content < 20 wt%; Woolley and Kempe, 1989) or > 30 vol% (regardless of silica content; Mitchell, 2005) carbonate minerals. They occur as both intrusive (e.g. dikes, plugs and sills; Rosatelli et al., 2000; Ying et al., 2017) and extrusive bodies (detailed discussion in Woolley and Church, 2005), and form predominantly with various alkaline silica-undersaturated (e.g., ijolite, phoscorite, foyaite etc.) and ultramafic

* Corresponding author at: University of Notre Dame, Department of Civil and Environmental Engineering and Earth Sciences, South Bend, IN, 46556, USA.
E-mail address: okaycimen@munzur.edu.tr (O. Çimen).

https://doi.org/10.1016/j.chemgeo.2019.07.015
Received 7 March 2019; Received in revised form 26 June 2019; Accepted 10 July 2019
Available online 13 July 2019
0009-2541/

rocks (e.g., Chen and Simonetti, 2013; Mitchell, 2005). Although exotic, carbonatites play an important role in our understanding of the chemical evolution of the asthenospheric and/or lithospheric mantle (e.g., Bell et al., 1982; Bell and Blenkinsop, 1987; Simonetti et al., 1998; Bell and Tilton, 2002; Hulett et al., 2016). They provide significant information on the nature of their mantle source due to their relatively high abundances of incompatible elements (e.g., Sr and Nd) and low viscosities, which help buffer their inherited isotope signatures against crustal contamination during their ascent to the surface (e.g., Jones et al., 2013 and references therein).

Carbonatites are found on all continents (Woolley and Kjarsgaard, 2008) including Antarctica (Hall et al., 1995; Worley et al., 1995). They are present in a number of tectonic settings (Woolley, 1989) but predominantly within intra-plate, continental rifts (e.g., East African Rift; Simonetti and Bell, 1993; Bell and Simonetti, 1996; Ernst and Bell, 2010), and less commonly within oceanic environments (e.g., Cape Verde Islands; Kogarko et al., 2009; Hoernle et al., 2002) and orogenic belts (e.g., Canadian Cordillera; Millonig et al., 2012; Chudy, 2013; Mitchell et al., 2017). On the basis of the radiogenic isotope systematics of young carbonatite complexes (< 200 Ma old) worldwide (for detailed review, Bell and Simonetti, 2010), it has been proposed that carbonatite melts are derived from a combination of mantle souces, including those characterized predominantly by EMI (Enriched Mantle I) and HIMU (high-μ; $^{238}U/^{204}Pb$) signatures (Zindler and Hart, 1986). A recent study by Hulett et al. (2016) conducted the intial investigation of the boron ($\delta^{11}B$) isotope compositions of carbonatite complexes worldwide ranging in age between ~2600 and 40 million years old. In summary, the study reported that several carbonatite occurrences < 300 million years in age display more positive $\delta^{11}B$ values (> −4‰) compared to those for several older carbonatite complexes, which are characterized by much lower $\delta^{11}B$ values (~ −7‰); the latter overlaping the boron isotopic composition for typical asthenospheric mantle (−7 ± 1‰; Chaussidon and Jambon, 1994). A more recent and detailed investigation of fresh (uncontaminated) mid-ocean ridge basalts (MORBs) from six ridge segments worldwide has established a mean value of −7.1 ± 0.9‰ (2σ standard deviation) for typical asthenospheric mantle (Marschall et al., 2017). The positive B isotope signatures from the younger carbonatite complexes were interpreted to reflect higher input of recycled crustal carbon within their mantle source region, which was linked to a change to modern-style plate tectonics and increased plume activity with increasing geological time (Hulett et al., 2016).

Given the B isotopic data for carbonatites from the Hulett et al. (2016) study, it is of interest to investigate further the $\delta^{11}B$ signatures for complexes located in different tectonic settings, and in particular for those situated in subduction/collision zones. Previous investigations of carbonatite complexes associated with subduction zones have suggested these are derived from the overriding, metasomatised sub-continental lithospheric mantle (SCLM) wedge (e.g., D'Orazio et al., 2007; Bonadiman et al., 2008; Deng et al., 2014). In this scenario, carbonatite magmas could result from melting of metasomatized SCLM that was modified by infiltration of high-flux REE- and CO_2-rich fluids derived from subducted marine sediments (e.g., Hou et al., 2006, 2015). In a recent study, Çimen et al. (2018) argue that the Miaoya carbonatite complex, which is located within a major collision-related tectonic zone in central China, was derived from an isotopically heterogeneous mantle source containing recycled crustal carbon on the basis of combined B, C, O, and radiogenic (Nd, Pb, and Sr) isotopic signatures.

With regards to alkaline magmatism associated with collisional settings, a suite of carbonatite complexes is located within such a tectonic environment in western Canada (Figs. 1 and 2). These fourteen carbonatite occurrences within seventeen alkaline centers in the Canadian Cordillera complexes were emplaced during extensional regimes within several orogenic cycles; in particular, the complexes younger than 360 Ma most likely formed during extension as a result of slab rollback (Millonig et al., 2012 and references therein; Rukhlov et al., 2018a, 2018b, 2019). The alkaline rocks and carbonatites from the eastern region of the Cordillera have been subdivided into three northwest trending belts, referred to as the Eastern, Central and Westerns Belts (Pell, 1987; Pell and Höy, 1989; see Mitchell et al., 2017 for details).

Recently, Millonig et al. (2012, 2013) and Mitchell et al. (2017) reported geochronological in-situ U-Th-Pb age determination of single zircons and baddeleyite (Millonig et al., 2013), which yield similar ages compared to zircons, and in-situ trace element and Sr-Nd isotope data for apatite from carbonatites within this region of western North America in order to understand better the chemical and geodynamic evolution of the mantle beneath this region. The geochronological results indicate that the carbonatitic magmatism in the southern Canadian Cordillera occurred intermittently during the Neoproterozoic (~800–700 Ma), Late Cambrian (~500 Ma) and Upper Devonian to Lower Carboniferous (~360–340 Ma; Millonig et al., 2012). Moreover, on the basis of the Sr and Nd isotopic composition of apatites, Mitchell et al. (2017) proposed carbonatite melt derivation from depleted sublithospheric mantle characterized by a mixed HIMU-EMI signature.

This study reports new and combined whole rock geochemical data, radiogenic (Sr, Nd, Pb) and stable (O and C) isotopic results together with the first $\delta^{11}B$ signatures for the Felix, Fir, Gum, and Howard Creek carbonatites. These are compared to the compositional and isotopic data for carbonatite samples from the Fen (Telemark, Norway), Jacupiranga (São Paulo State, Brazil) and Chipman Lake (Ontario, Canada). These latter carbonatite complexes did not form in a collision-type tectonic environment, but rather are associated with continental rifting events and/or mantle plume activity. Comparison of all of these new data with existing data for worldwide occurrences, will help to better evaluate the mantle source(s) and the petrogenetic link (if any) between “orogenic” and anorogenic carbonatite compexes. Finally, given the complex tectono-metamorphic history of the geological region investigated here, this study provides an opportunity to evaluate the robustness and behavior of the B isotope system as applied to carbonatite complexes.

2. Geological setting and sample descriptions

2.1. Blue river carbonatites, British Columbia, Canada

The Canadian Cordillera is located on the western margin of the North American continent and is commonly subdivided into five west to east tectonic belts based on their rock associations, metamorphic grade and structural style (Fig. 1), and these are: the Insular Belt, the Coast Plutonic Complex, the Intermontane Belt, the Omineca Crystalline Belt, and the Rocky Mountain Trench (e.g., Monger and Price, 2002; Millonig et al., 2012; Chudy, 2013). The Blue River carbonatites and associated alkaline rocks occur within the central belt of the eastern Cordillera, which is located west of the Rocky Mountain Trench within the Omineca Crystalline Belt (e.g., Pell and Höy, 1989; Millonig et al., 2012; Chudy, 2013). There are various carbonatite occurrences in the Blue River area (Fig. 2), which occur as small (100 m) discontinuous outcrops (e.g., Pell, 1987; Mitchell et al., 2017) in the form of sill-like bodies and lenses. These have intruded Late Proterozoic strata (e.g., Horsethief Creek Group; Pell and Simony, 1987; Chudy, 2013; Fig. 2) during rifting and extensional episodes in the Late Cambrian (e.g., Felix and Little Chiago) and Devono-Mississippian times (e.g., Fir; Gorham et al., 2009; Serpentine Creek and Mud Lake; Millonig et al., 2012), prior to deformation and metamorphism associated with the late Jurassic Columbian orogeny (Millonig et al., 2013 and references therein).

The tectonic belts within the Canadian Cordillera have been metamorphosed to different degrees (Fig. 1). For example, igneous and sedimentary rocks belonging to the Omineca Belt experienced subgreenschist to amphibolite facies conditions, whereas the metamorphism in the Foreland Belt did not exceed greenschist facies conditions (e.g., Read et al., 1991; Millonig et al., 2012). In detail, the Blue

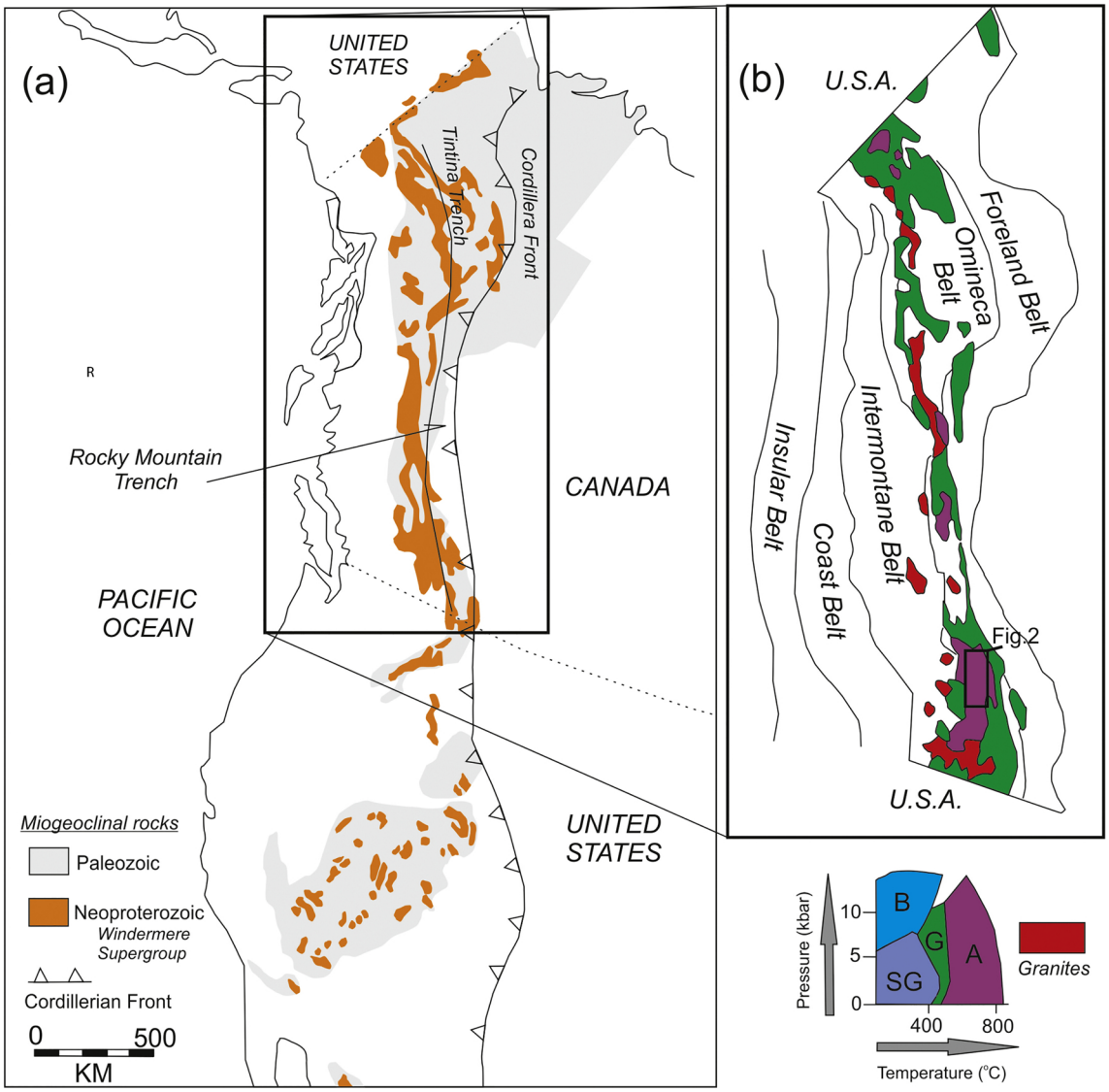

Fig. 1. Neoproterozoic and Paleozoic miogeoclinal rocks in western North America (a). Simplified metamorphic map of the Canadian Cordillera (b). As indicated in the pressure-temperature diagram, Sg: Sub-greenschist facies, G: Greenschist facies, A: Amphibolite facies. Both figures modified after Millonig et al. (2012).

River region has been deformed and metamorphosed during at least three tectono-metamorphic events, which have been identified using stratigraphic correlations in the Horsethief Creek group strata (Sevigny and Simony, 1989; Chudy, 2013). There are localized multiple metamorphic events that took place between ~160 and 56 Ma in the Blue River area based on previous geochronological studies (Millonig et al., 2013 and references therein). The earliest, major event occurred during the Early Cretaceous (140–111 Ma) as evidenced by radiometric ages recorded for pelitic schists and deformed pegmatites (Chudy, 2013 and references therein). Subsequently, a thermal event accompanied partial melting of metapelites that produced *syn*-and post-kinematic peraluminous granites at ~100 Ma and 63 Ma, respectively (Sevigny et al., 1989). The cooling of the Blue River region occurred between 75 and 54 Ma based on amphibole and mica K-Ar and Ar-Ar ages from the Omineca Crystalline Belt and Mica Creek Area (Millonig et al., 2013 and references therein).

Mitchell et al. (2017) document that the Blue River area carbonatites contain both calcite and dolomite and these exhibit a wide range of textures and compositions, which are the result of re-crystallization during their tectono-metamorphic evolution. The latter includes development of mylonitic shear zones and the redistribution of minor and accessory phases parallel to the foliation (Mitchell et al., 2017). Consequently, the petrogenetic context of the observed parageneses have been significantly modified for the majority of the carbonatite sills, in particular for the thinner (< 1 m) calcitic occurrences (Mitchell et al., 2017). In contrast, the thicker dolomitic carbonatite sills present at Fir preserve some magmatic features that permit investigation of the evolution of this system (Chudy, 2013). For example, Mitchell et al. (2017) report that relics of magmatic textures are still present in sections of the carbonatite that escaped pervasive shearing and dynamic re-crystallization. In particular, they describe the presence and intact paragenetic relations of three calcite and dolomite generations, which were identified by cathodoluminescence microscopy and microprobe analysis. The three generations include: 1- Mg-depleted, 2- peak-metamorphic, and 3- retrograde calcite. Detailed petrographic descriptions and observations are documented in Mitchell et al. (2017) and are briefly summarized here. The Fir carbonatite covers an area of 1 km by 4.5 km and consists of isoclinal recumbent folds of < 5 m to 90 m thick sills with strike lengths of 50 m to 1100 m (Kulla and Hardy, 2015). The Fir carbonatite consists of dolomite with abundant fluorapatite (5–20 vol%) and Na-Ca amphiboles (5–20 vol%; Fig. 3); accessory phases include phlogopite, zircon, pyrrhotite, ilmenite, magnetite, ferrocolumbite, pyrochlore supergroup minerals, fersmite, thorite, nioboaeschynite and monazite. Three main mineralogical facies are based

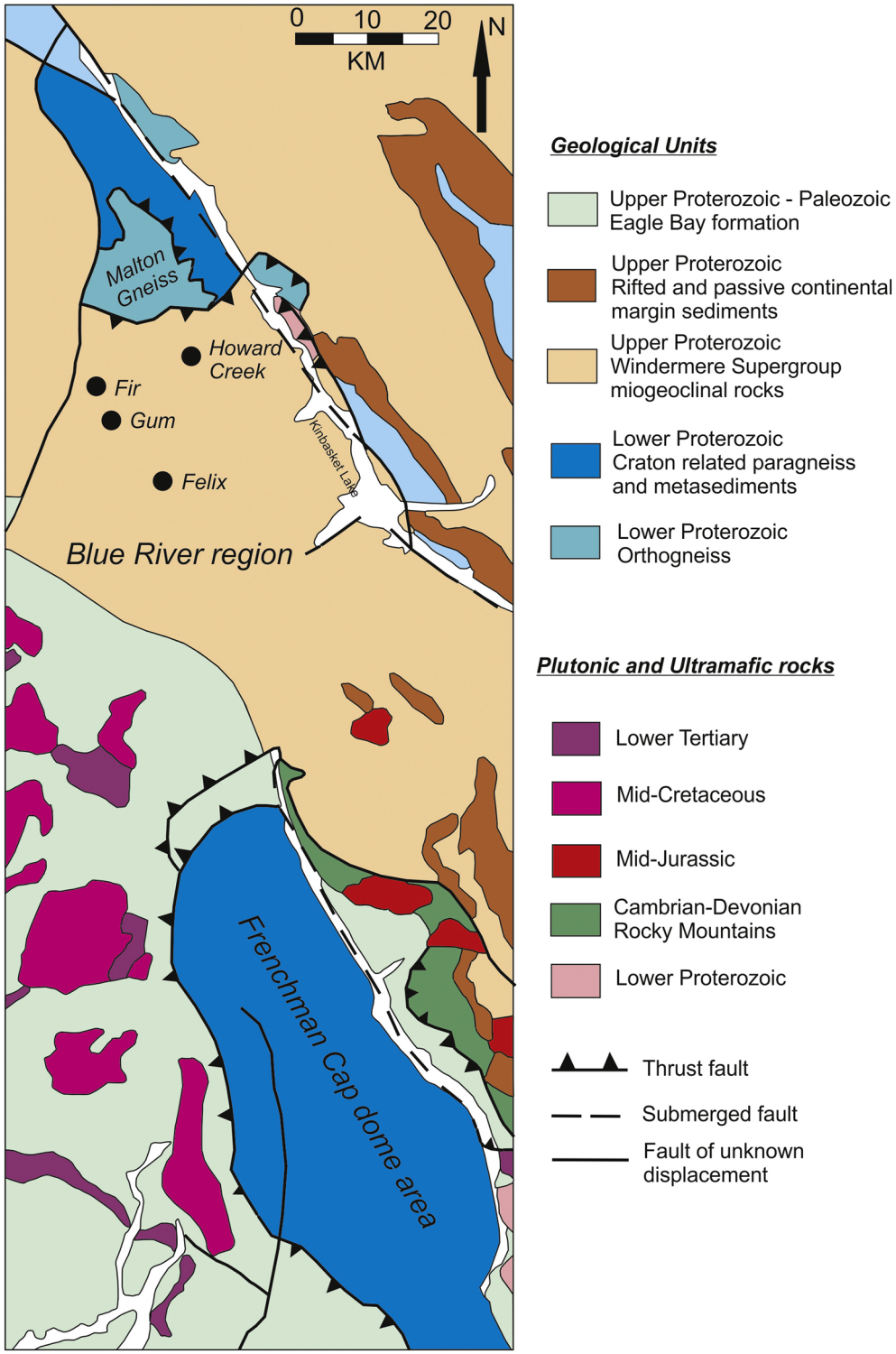

Fig. 2. Geological map of the Blue River region and Frenchman Cap dome area (modified from Millonig et al., 2012). (For interpretation of the references to colour in this figure legend, the reader is referred to the web version of this article.)

on the amphibole composition and the Nb-Ta oxide minerals, and are as follows: 1- anchimonomineralic facies essentially devoid of accessory phases containing ferrocolumbite, 2- a winchite (and ferrocolumbite) facies (Fig. 3), and 3- a katophorite (and pyrochlore) facies. The Fir samples investigated here are from both the winchite (FIR-W) and katophorite (FIR-K) facies. The Fir complex consists ~5 vol% of calcite carbonatite that occurs solely with the katophorite facies proximal to the center of the sills. The Howard Creek carbonatites occur as a series of thin isoclinally folded sills (Pell, 1987), and the majority consist of equigranular calcite with rounded apatite crystals (Fig. 3). They also contain phlogopites, rounded (up to 2 mm) olivine crystals (Fo: 83–88) with inclusions of magnetite and apatite, diopside, plus late stage magnetite, ilmenite and pyrite. The Gum carbonatite sill, which is up to 10 m thick and several tens of meters in length, is apatite-rich calciocarbonatite. The latter is locally wrapped around neighbouring leucocratic amphibolites, and exhibits bedded-to-slaty cleavage. The

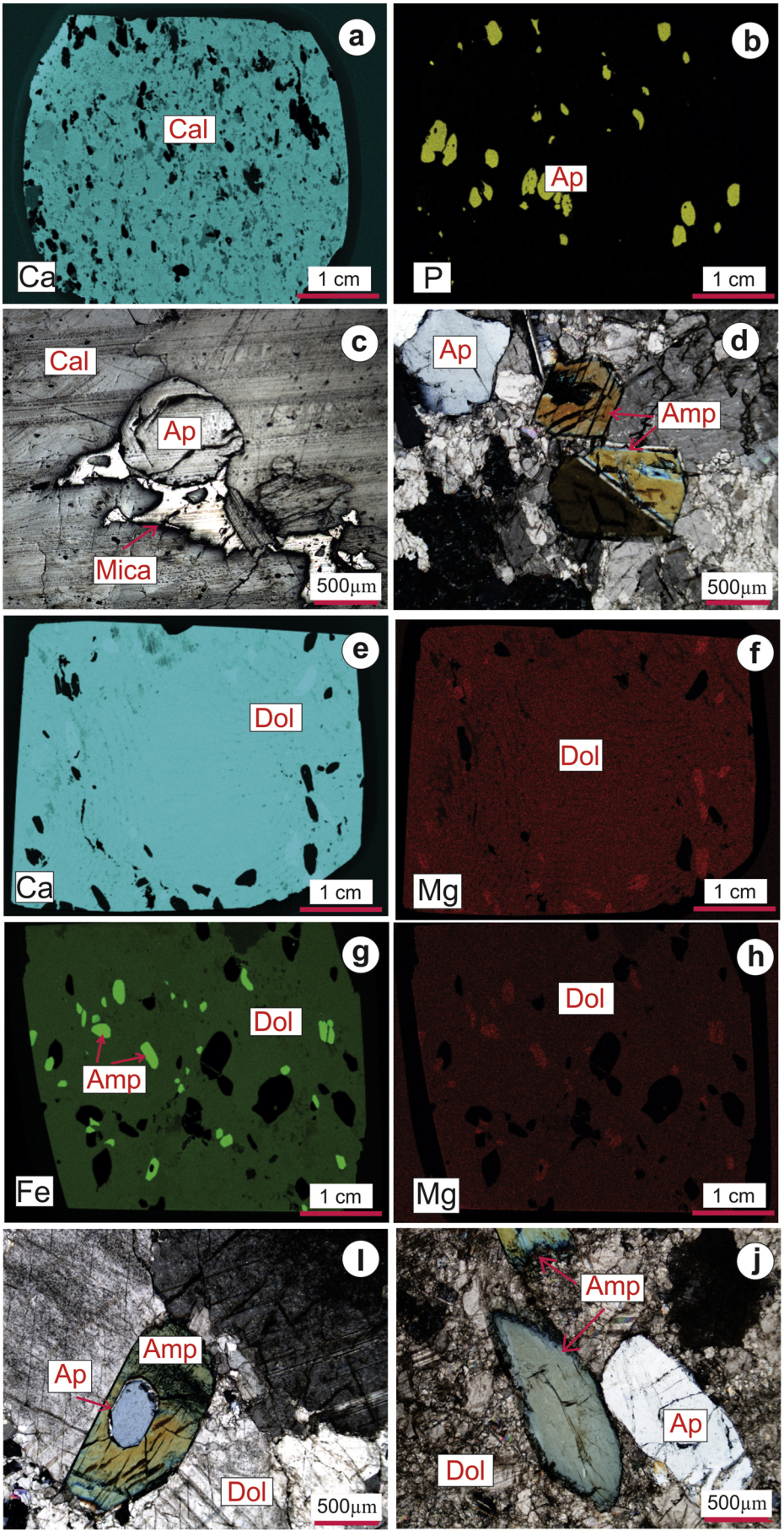

(caption on next page)

Fig. 3. Micro-XRF and thin section images for samples GUM-BC (a-b); HW-CR (c-d); FIR-K (e–f) and FIR-W (g to j) illustrating presence of medium-to-coarse-grained calcite (Cal), dolomite (Dol), apatite (Ap), winchite amphibole (Amp) and mica.

carbonatite contains calcite, apatite, and amphibole in similar amounts, and minor and accessory phases include phlogopite, magnetite, zircon and pyrochlore. The Felix carbonatite forms an extensive sill-like body (~10 × 200 m) and its geological setting is complex and has not been thoroughly investigated. The carbonatite sill exhibits modal layering of magnetite and has been, in parts, complexly folded. The mineralogy consists of large rounded apatite crystals set in an equigranular matrix of calcite with very small exsolved dolomite crystals; olivine and magnetite occur as trace minerals.

2.2. Fen carbonatite, Telemark, Norway

The Fen carbonatite is located in Telemark, southeast Norway about 20 km west of the late Paleozoic Oslo rift (Andersen and Taylor, 1988). In this region, the Precambrian gneisses and amphibolites represent the host rocks to the Fen carbonatite. This complex includes a composite central magmatic system and several satellite intrusions (Andersen, 1987 and references therein). The most abundant magmatic rocks consist of carbonatites (60%) and associated intrusive silicate rocks (< 20%), with the remainder consisting of metasomatized country rocks (Andersen and Taylor, 1988). Based on a Pb-Pb whole rock isochron age of 539 ± 14 Ma (Andersen and Taylor, 1988) and two consistent $^{40}Ar/^{39}Ar$ ages of 583 ± 15 Ma (Meert et al., 1998), the Fen carbonatite was formed in Cambrian or latest Neoproterozoic. Dahlgren (1994) has reported a Rb-Sr isochron age of 578 Ma for this complex, which is consistent with the ages cited above. The calcite-dolomite carbonatite is composed of primary calcite, dolomite, apatite, pyrite, magnetite and columbite with accessory quartz, baryte, pyrochlore, fluorite and REE fluorocarbonates (Marien et al., 2018). This investigation reports new compositional and isotope data and first boron isotope signatures for carbonate separates for two carbonatite samples taken from the Hydro Quarry.

2.3. Chipman Lake carbonatite, Ontario, Canada

The Chipman Lake carbonatite occurrence is located ~350 km northeast of Thunder Bay, Ontario and includes a series of dikes intruding rocks of the Archean Wabigoon Sub-province within the Superior Province (Platt and Woolley, 1990). The small dikes (< 1 m thick) associated with marginal fenites crop-out at the southern end of Chipman Lake (Platt and Woolley, 1990). The carbonates from these carbonatites are composed of dolomite, ferroan dolomite- to- ankerite, with minor calcite (Buckley and Woolley, 1990). Based on cathodoluminescence studies (Platt and Woolley, 1990), there are two major carbonate phases within some dikes that consist of an early dolomitic phase brecciated by younger ankeritic carbonate. The age of the Chipman Lake carbonatite is considered as Mesoproterozoic based on a K-Ar age of 1022 ± 31 Ma (Sage, 1985) for amphibole from fenite. We report here new compositional and isotopic data and first boron isotope compositions for carbonate separated from a carbonatite dike located on the south shore of Chipman Lake.

2.4. Jacupiranga carbonatite, São Paulo State, Brazil

The Jacupiranga carbonatite, which is located in southeastern Brazil, was emplaced into a Late Precambrian mica schist and syntectonic granodiorite belt (Roden et al., 1985; Huang et al., 1995). The time of emplacement occurred in Early Cretaceous based on Rb-Sr and K-Ar ages of 131 ± 3 Ma (Roden et al., 1985) and 130 ± 5 Ma (Amaral, 1978), respectively. In this alkaline complex, five distinct carbonatite intrusions and two separate intrusive stages of silicate rocks have been recognized, which consist of syenites, pyroxenites, peridotites, ijolites and fenite (Huang et al., 1995 and references therein). The Jacupiranga carbonatites consist mainly of calcite, dolomite, apatite, forsterite, phoscorite, and pyrochlore (Costanzo et al., 2006). Roden et al. (1985) and Huang et al. (1995) reported that the initial Sr, Nd and Pb isotope ratios from the Jacupiranga carbonatite complex are similar to those of basalts from several nearby alkaline complexes, including those from Parana (high-Ti), the Walvis Ridge and Tristan da Cunha; hence, providing evidence for derivation from similar mantle source regions. This investigation reports new compositional and isotopic data and the first boron isotope composition for carbonate separated from carbonatite within the main pit.

3. Analytical methods

3.1. μXRF mapping

Qualitative elemental maps (Fig. 3; Si, Al, Mg, K, Ti, Ca, Fe) were produced for ~100 μm thick petrographic thin sections using an Edax Orbis micro-XRF instrument at the Center for Environmental Science and Technology (CEST), University of Notre Dame. The mapping was conducted overnight (~12 h) and the X-ray conditions of the instrument were as follows: amplifier time 12.8 μs, fluorescent energy 32 kV, beam size 30 μm, matrix 512 × 400, Dwell time of 200 ms, spectrum map 32-Bit.

3.2. Electron microprobe analyses

The major and minor element concentrations (Table 1) of carbonate grains were determined by using a CAMECA SX-50 electron microprobe at the University of Notre Dame. The instrument was operated with a 15 kV of accelerating voltage, 10 nA beam current, and 15 μm beam diameter. The following standards were used for calibration: TAP for Mg, PETJ for Ca, Sr, Mn, and LIFT for Fe. The peak and background counting times were 30 s for Mn and Fe, 25 s for Sr, 15 s for Mg, and 5 s for Ca.

3.3. Trace element determinations

The carbonate grains/fragments for determination of trace element concentrations (Table 2) were hand-picked using a binocular microscope in a class 1000 clean room facility at the Midwest Isotope and Trace Element Research Analytical Center (MITERAC), University of Notre Dame. Details for analytical procedures employed here are included within the appendix.

3.4. Stable (B, C, O) and radiogenic (Sr, Pb, Nd) isotope analyses

The $\delta^{18}O$ and $\delta^{13}C$ isotope data (Table 3) for carbonate separates were obtained using a Delta V Advantage isotope ratio mass spectrometer housed within CEST (University of Notre Dame). The chemical purification and isotope ratio measurement procedures for boron isotope analyses of carbonate separates (Table 3) employed here are from Hulett et al. (2016). The B, Sr, Pb and Nd isotope analyses reported in Tables 3, 4 and 5 were conducted using a NuPlasma II MC-ICP-MS instrument at University of Notre Dame. Details for all analytical procedures employed for both the stable and radiogenic isotope measurements are provided within the appendix.

Table 1
Major and minor element abundances (wt%) for carbonates from the Blue River carbonatite samples.

Sample/point	MgO	FeO	MnO	CaO	SrO	SUM
FIR-W-1	16.57	6.22	0.88	29.67	0.51	53.84
FIR-W-2	16.56	6.13	0.89	29.80	0.59	53.96
FIR-W-3	16.65	6.29	0.87	29.63	0.60	54.05
FIR-W-4	16.26	6.90	0.85	29.98	0.63	54.61
FIR-W-5	16.31	6.85	0.93	29.39	0.53	54.01
FIR-W-6	16.82	6.20	0.86	29.68	0.52	54.09
FIR-W-7	17.01	6.06	0.86	29.34	0.48	53.75
FIR-W-8	16.50	6.58	0.97	29.65	0.54	54.23
FIR-W-9	0.03	0.06	0.07	54.55	1.15	55.85
FIR-W-10	0.03	0.04	0.07	54.33	1.04	55.51
FIR-W-11	0.02	0.06	0.03	54.54	1.28	55.92
FIR-W-12	16.63	6.17	0.90	29.92	0.50	54.11
FIR-W-13	16.54	6.36	0.88	29.56	0.51	53.85
FIR-W-14	16.71	6.19	0.88	29.55	0.56	53.90
FIR-W-15	16.72	6.05	0.86	29.68	0.40	53.70
FIR-K-1	16.18	7.10	0.96	29.52	0.66	54.42
FIR-K-2	16.04	6.86	0.88	29.78	0.54	54.11
FIR-K-3	16.06	6.86	0.90	29.31	0.52	53.64
FIR-K-4	15.97	7.04	0.91	29.80	0.68	54.40
FIR-K-5	16.03	6.89	0.94	29.97	0.63	54.45
FIR-K-6	16.14	7.06	0.91	29.31	0.56	53.97
FIR-K-7	15.93	7.31	0.92	29.36	0.61	54.12
FIR-K-8	16.00	7.17	0.90	29.84	0.66	54.57
FIR-K-9	0.01	0.08	0.05	54.55	1.55	56.25
FIR-K-10	0.03	0.04	0.02	55.02	1.25	56.37
FIR-K-11	0.04	0.15	0.07	54.68	1.02	55.96
FIR-K-12	16.04	7.54	0.89	29.81	0.68	54.96
FIR-K-13	15.99	7.18	0.90	29.33	0.64	54.03
FIR-K-14	16.18	7.10	0.94	29.43	0.56	54.20
FIR-K-15	15.72	7.44	0.93	29.30	0.68	54.06
GUM-1	1.24	1.56	0.66	56.61	1.56	61.62
GUM-2	1.58	1.77	0.70	57.17	1.49	62.71
GUM-3	15.75	7.18	0.88	30.15	0.58	54.55
GUM-4	15.39	7.54	1.02	29.95	0.71	54.61
GUM-5	15.60	7.38	0.91	29.90	0.59	54.38
GUM-6	1.14	1.50	0.67	56.37	1.57	61.25
GUM-7	1.15	1.45	0.63	56.96	1.37	61.57
GUM-8	1.12	1.45	0.58	57.74	1.64	62.53
GUM-9	1.28	1.50	0.63	58.39	1.45	63.26
GUM-10	1.20	1.53	0.66	58.24	1.44	63.08
GUM-11	1.12	1.52	0.64	58.90	1.72	63.90
GUM-12	1.45	1.70	0.72	57.20	1.70	62.76
GUM-13	1.32	1.56	0.64	57.63	1.65	62.80
HW-CR-1	2.22	0.34	0.16	49.15	0.59	52.46
HW-CR-2	2.58	0.36	0.20	60.11	0.56	63.81
HW-CR-3	2.71	0.34	0.20	59.93	0.53	63.71
HW-CR-4	2.62	0.37	0.13	60.09	0.59	63.81
HW-CR-5	2.01	0.32	0.16	58.74	0.58	61.80
HW-CR-6	2.49	0.41	0.15	59.15	0.57	62.76
HW-CR-7	2.57	0.38	0.12	59.29	0.63	63.00
HW-CR-8	1.80	0.29	0.14	61.72	0.57	64.51
HW-CR-9	2.68	0.27	0.18	60.18	0.65	63.95
FLX-1	18.52	3.71	0.29	31.48	0.24	54.23
FLX-2	18.40	3.71	0.30	31.04	0.30	53.75
FLX-3	3.44	1.28	0.27	57.82	0.59	63.40
FLX-4	18.73	3.72	0.26	32.04	0.33	55.06
FLX-5	2.84	1.08	0.23	57.09	0.60	61.84
FLX-6	10.31	2.54	0.29	43.77	0.45	57.36
FLX-7	2.25	0.86	0.21	48.93	0.67	52.91
FLX-8	18.53	3.59	0.29	31.88	0.22	54.51
FLX-9	18.61	3.78	0.23	32.05	0.31	54.98
FLX-10	3.80	1.30	0.29	58.70	0.61	64.70
FLX-11	3.36	1.14	0.24	56.52	0.54	61.79
FLX-12	2.99	1.22	0.26	56.95	0.62	62.04
FLX-13	2.57	1.01	0.25	54.85	0.52	59.20

4. Results

4.1. Major, minor and trace element geochemistry

Major and minor element concentrations for carbonate separates from the Blue River carbonatite samples are listed in Table 1. The CaO and MgO wt% concentrations reported here indicate that there are two main carbonates, which correspond to compositions of calcite and dolomite (Fig. 4a). With the exception of the sample from Howard Creek (which contains only calcite), the remaining samples include both calcite and dolomite.

The trace element and B contents for carbonate separates from the carbonatites investigated here are listed in Table 2. A majority of the B abundances are ≤1 ppm (except for Felix at 3.06 ppm), which are consistent with those from fresh (unaltered) mid-ocean ridge basalts (e.g., MORBs; Marschall et al., 2017; Spivack and Edmond, 1987; Wunder et al., 2005), and boron concentrations reported for a majority of carbonatites worldwide (Hulett et al., 2016; Çimen et al., 2018). The total rare earth element (TREE) concentrations determined here for the Blue River carbonatites vary between 215 and 1483 ppm, and the corresponding chondrite-normalized (CN)-REE patterns display variable degrees of enrichment in light (LREEs) over heavy (HREEs; $La/Lu_{(CN)}$ = 32.3–86.5; Table 2; Fig. 5). Fig. 5 also illustrates and compares the CN-REE patterns obtained for the dolomite carbonatites from Fir to previous studies (Chudy, 2013) and those for apatites from various Blue River carbonatites (Mitchell et al., 2017).

4.2. Boron, carbon, and oxygen isotope data

Oxygen and carbon stable isotope data obtained for carbonate separates from the Blue River carbonatites are listed in Table 3 and illustrated in Fig. 6. The $\delta^{18}O_{SMOW}$ (‰) and $\delta^{13}C_{PDB}$ (‰) values vary between +9.14‰ and + 9.62‰ and − 5.37‰ and − 4.85‰, respectively, and plot within the field for "primary igneous carbonatites (PIC)" ($\delta^{18}O$ ~ +6‰ to +10‰ and $\delta^{13}C$ ~ −4‰ to −8‰; Keller and Hoefs, 1995; Fig. 6). In addition, the samples from Fen ($\delta^{18}O_{SMOW}$ = 8.94‰ and 9.28‰; $\delta^{13}C_{PDB=}$ − 4.90‰ and-4.72‰) also fall within the PIC field, whereas the sample from Chipman Lake ($\delta^{18}O_{SMOW}$ = 10.54‰; $\delta^{13}C_{PDB=}$ − 4.52‰) plots slightly to the right of the PIC box, and that from Jacupiranga ($\delta^{18}O_{SMOW}$ = 16.55‰; $\delta^{13}C_{PDB=}$ − 5.62‰) plots much further away to the right of the PIC with an enriched O isotope composition.

The first-reported $\delta^{11}B$ (‰) values for the carbonate separates from the Blue River region carbonatites range between −8.67‰ and − 2.47‰ and are listed in Table 3. The samples from Gum, Howard Creek, and Felix are characterized by negative $\delta^{11}B$ values, between −8.67‰ and − 6.36‰, which overlap (given their associated uncertainties) the range of values for typical asthenospheric (MORB) mantle of ~ −7.1 ± 0.9‰ (Marschall et al., 2017). The $\delta^{11}B$ signatures of carbonate separates from the Fir carbonatites (−3.98 and − 2.47‰) are slightly higher than the remaining samples, and overlap the B isotope compositions for young (< 300 Ma old) carbonatites worldwide (Hulett et al., 2016; Fig. 7). Moreover, while the $\delta^{11}B$ values for the carbonate samples from Fen (−7.12 and − 9.79‰) and Chipman Lake (−8.48‰) also overlap that for typical asthenospheric mantle, the carbonate sample from Jacupiranga yields a much higher value of +0.62‰ (Fig. 7).

4.3. Sr, Pb, and Nd isotope data

The new Sr, Nd, and Pb isotope data for carbonate separates from the Blue River carbonatites are listed in Tables 4 and 5 and shown in Figs. 7, 8, and 9. The ages of ~340 Ma (Serpentine Creek carbonatite) and 497 Ma (Felix carbonatite), which are both from Millonig et al. (2012) for the Blue River carbonatites, have been adopted for the calculation of initial ratios. Ages of 578 Ma (Dahlgren, 1994), 1022 Ma (Sage, 1985) and 131 Ma (Roden et al., 1985) have been adopted for the samples from Fen, Chipman Lake, and Jacupiranga for their respective age corrections of measured isotope ratios.

Given the low $^{87}Rb/^{86}Sr$ values (0 to ~0.004) for all carbonate samples investigated here with the exception of the sample from Jacupiranga (0.12), the magnitude of the age correction of the measured

Table 2
Trace element concentrations (ppm) for carbonate separate from the carbonatite samples.

	FIR-W	FIR-K	GUM	HW-CR	FLX	FEN-1	FEN-2	CHP-LK	JC-PR
Latitude			*51.1065 N*		*5.2838 N*			*46.5438 N*	*24.7023 S*
Longitude			*119.3049 W*		*9.2646 E*			*83.7782 W*	*48.0076 W*
B	0.21	0.15	0.39	0.52	3.06	0.36	0.80	0.24	0.26
Sc	1.12	1.17	1.36	2.71	2.54	0.83	1.05	7.33	0.28
V	0.21	0.38	0.58	0.69	1.28	3.70	3.36	1.15	20
Cr	0.08	*b.d.l.*	0.21	*b.d.l.*	0.51	*b.d.l.*	*b.d.l.*	0.42	0.41
Co	4.7	6.1	1.04	0.91	4.1	0.11	0.14	4.4	22
Ni	1.09	0.71	2.04	1.91	22	1.52	2.17	1.02	9.1
Cu	0.70	0.54	1.22	0.57	2.34	0.27	0.31	0.70	55
Zn	29	29	8.7	3.4	8.3	5.5	9.4	25	11
Rb	0.01	0.03	0.02	0.08	1.00	0.28	0.81	0.24	6.8
Sr	1268	876	899	732	995	517	673	502	161
Y	18	17	103	41	50	24	33	16	6.5
Zr	0.31	0.26	0.19	0.31	0.12	0.40	0.26	0.57	1.17
Nb	2.8	0.22	1.04	0.23	0.19	0.41	1.23	12	0.03
Mo	0.55	0.34	0.41	0.11	0.10	0.09	0.11	0.40	3.71
Cs	0.01	0.01	*b.d.*	0.01	0.03	0.02	0.02	0.01	0.14
Ba	10.8	5.6	268	22	16	23	37	20	37
La	75	71	389	142	142	72	107	68	19
Ce	80	122	711	276	313	158	232	197	34
Pr	8.6	13	64	30	36	17	24	24	3.5
Nd	34	53	216	117	148	64	90	94	14
Sm	5.60	8.85	36	21	25	10.6	15	18	2.5
Eu	1.7	2.5	9.6	6.0	7.4	3.1	4.4	5.0	0.64
Gd	4.1	6.6	24	16	20	8.1	11.4	12.5	2.2
Tb	0.48	0.77	2.9	1.9	2.4	1.03	1.45	1.39	0.27
Dy	2.3	3.52	14.5	9.4	11.8	5.2	7.3	5.8	1.30
Ho	0.42	0.62	2.7	1.7	2.1	1.01	1.37	0.88	0.25
Er	0.92	1.29	6.1	3.6	4.7	2.2	3.2	1.56	0.52
Tm	0.11	0.14	0.76	0.42	0.56	0.28	0.40	0.16	0.06
Yb	0.68	0.82	4.5	2.4	3.4	1.81	2.5	0.80	0.35
Lu	0.09	0.11	0.64	0.33	0.46	0.26	0.36	0.09	0.04
W	0.02	0.02	0.06	0.06	0.14	0.05	0.16	0.08	0.09
Pb	1.69	1.35	1.50	4.3	2.1	17	6.6	0.62	0.23
Th	0.27	1.19	0.67	4.2	1.04	19	3.4	1.27	0.52
U	0.15	0.17	0.24	0.57	0.28	5.6	1.10	0.18	0.12

b.d.l. = below detection limit.

Table 3
C, O, and B isotope data for carbonate separates from the carbonatite samples investigated here.

Sample	$\delta^{13}C$ (‰)	uncertainty	$\delta^{18}O$ (‰)	uncertainty	$\delta^{11}B$ (‰)[a]
FIR-W	−5.06	0.03	9.21	0.03	−3.98
FIR-K	−4.85	0.03	9.35	0.03	−2.47
GUM	−5.37	0.02	9.61	0.03	−8.67
HW-CR	−5.29	0.04	9.14	0.06	−6.36
FLX	−4.98	0.05	9.62	0.09	−8.38
FEN-1	−4.72	0.03	9.28	0.02	−7.12
FEN-2	−4.90	0.02	8.94	0.02	−9.79
CHP-LK	−4.52	0.03	10.54	0.03	−8.48
JC-PR	−5.62	0.52	16.55	0.81	0.62

[a] Uncertainty associated with B isotope ratios is ± 0.5‰ (2 s level) based on replicate analyses of coral in-house standard (see text for details).

$^{87}Sr/^{86}Sr$ ratios (0.70258 to 0.70442) is minimal (Table 4). The initial Sr isotope ratios (0.70256 to 0.70442) for the Blue River carbonatites fall within the range of values previously reported for apatite for several complexes examined here (Howard Creek = 0.70310–0.70354; FIR-K = 0.70290–0.70291 and FIR-W = 0.70280–0.70285; Gum = 0.70390–0.70404, and Felix = 0.70338–0.70346; Mitchell et al., 2017). In comparison, the carbonatite sample from Chipman Lake is characterized by the lowest initial $^{87}Sr/^{86}Sr$ (0.70256) ratio, whereas the initial Sr isotope compositions (0.70306–0.70309) for the carbonate samples from Fen are identical (given their associated uncertainties), and overlap those reported in previous studies for this complex (Andersen, 1987; Fig. 8). In contrast, the initial $^{87}Sr/^{86}Sr$ ratio (0.70382) for the carbonate from Jacupiranga is much lower compared to those from previous studies (e.g., Roden et al., 1985; Huang et al., 1995; Beccaluva et al., 2017; Fig. 8).

The $^{147}Sm/^{144}Nd$ ratios vary between ~0.10 and ~0.12 for all carbonate samples investigated here, which results in corresponding, calculated initial $^{143}Nd/^{144}Nd$ ratios that range between 0.51136 and 0.51269 (Table 4). The corresponding $\varepsilon_{Nd(t)}$ values (Table 4, Fig. 8) overlap those reported for apatite from the equivalent complexes examined by Mitchell et al. (2017), and the comparison is shown in Fig. 8a. The sample from Chipman Lake has the lowest initial $^{143}Nd/^{144}Nd$ (0.511356) ratio that corresponds to a $\varepsilon_{Nd(1022Ma)}$ value of +0.7, whereas the sample from Jacupiranga has the highest initial $^{143}Nd/^{144}Nd$ (0.51269) ratio that results in a $\varepsilon_{Nd(131Ma)}$ value of +4.4 (Fig. 8).

The initial Pb isotope values for carbonate grains from the Blue River carbonatites define a rather large range for $^{206}Pb/^{204}Pb$ (21.14–107.42), $^{207}Pb/^{204}Pb$ (15.87–20.42), and $^{208}Pb/^{204}Pb$ (39.34–41.39; Table 5). In particular, the carbonate sample from Fir (FIR-W) has significantly higher initial $^{206}Pb/^{204}Pb$ and $^{207}Pb/^{204}Pb$ ratios than the remaining samples (Table 5). Moreover, the carbonate samples from Fen, Chipman Lake and Jacupiranga have lower initial Pb isotope ratios (i.e., $^{206}Pb/^{204}Pb$ = 16.89–21.38) compared to the remaining complexes from the Blue River region (Fig. 9).

5. Discussion

5.1. Carbonate composition and metamorphism

The carbonate samples from the Blue River region (British

Table 4
Sr and Nd isotope data for carbonate separates from the carbonatite samples investigated in this study.

Sample	Rb (ppm)	Sr (ppm)	$^{87}Rb/^{86}Sr$	$^{87}Sr/^{86}Sr$	2σ	$^{87}Sr/^{86}Sr(i)$	Sm (ppm)	Nd (ppm)	$^{147}Sm/^{144}Nd$	$^{143}Nd/^{144}Nd$	2σ	$^{143}Nd/^{144}Nd$ (*i*)	εNd(*t*)
FIR-W	0.01	1268	0.00003	0.70297	0.00001	0.70297	5.6	34	0.10	0.51272	0.00001	0.51249	5.7
FIR-K	0.03	876	0.00009	0.70297	0.00001	0.70297	8.9	53	0.10	0.51272	0.00001	0.51250	5.8
GUM	0.02	899	0.00006	0.70442	0.00002	0.70442	35	216	0.10	0.51233	0.00001	0.51211	−1.8
HW-CR	0.08	732	0.0003	0.70322	0.00001	0.70322	21	117	0.11	0.51259	0.00001	0.51235	2.9
FLX	1.00	995	0.003	0.70379	0.00001	0.70377	25	148	0.10	0.51243	0.00001	0.51209	1.9
FEN-1	0.28	517	0.0016	0.70308	0.00001	0.70306	10.6	64	0.10	0.51248	0.00001	0.51210	4.0
FEN-2	0.81	673	0.003	0.70312	0.00001	0.70309	15	90	0.10	0.51245	0.00001	0.51207	3.4
CHP-LK	0.24	502	0.0014	0.70258	0.00001	0.70256	18	94	0.12	0.51214	0.00001	0.51136	0.7
JC-PR	6.75	161	0.12	0.70404	0.00001	0.70382	2.5	14.4	0.10	0.51278	0.00001	0.51269	4.4

Please see text for details in relation to age correction. $^{87}Rb/^{86}Sr$ and $^{147}Sm/^{144}Nd$ values were calculated based on ICP-MS-determined elemental abundances and are associated with relative uncertainties of between 3 and 5% (2σ level).

Columbia, Canada) are characterized by the presence of both calcite and dolomite, with the exception of Howard Creek that only contains calcite (Table 1; Fig. 4a). Based on the major and minor element concentrations for carbonates reported here (Fig. 4), there are no clear compositional trends that may be attributed to closed system fractional crystallization involving a single parental melt with the possible exceptions of the samples from Fir and Felix. This is perhaps not an unexpected result given that these carbonatites have been subjected to tectono-metamorphic events subsequent to their emplacement. However, as stated earlier, the thicker complexes such as Fir and Felix may better preserve their inherent original compositional variations (as discussed in Mitchell et al., 2017). For example, the negative array defined by the MgO vs. FeO wt% abundances for the carbonates from samples FIR-W and FIR-K may reflect combined early amphibole and apatite fractional crystallization (Figs. 3 and 4c). Overall, the data shown in Fig. 4 most probably indicates that either multiple primary melts were involved in the petrogenesis of the Blue River carbonatite complexes, or the major element compositions were perturbed by the complex tectono-metamorphic history of the area. Despite having experienced various degrees of deformation and metamorphism, the major element compositions for the Blue River carbonates define similar trends and compositions compared to the calcitic and dolomitic carbonatites from the Spitskop complex, South Africa (Fig. 4; Harmer, 1999). The latter complex is a classic example of a carbonatite system yielding phases characterized by a bimodal distribution of carbonate minerals (calcite and dolomite). Given their distinct and variable radiogenic isotope compositions, Harmer (1999) argued that the calcio- and dolomitic carbonatites from Spitskop were not related to a single parental carbonatite magma, nor the products of liquid immiscibility.

Melting experiments conducted at pressures between 30 and 100 kbar of carbonated peridotite have produced low degree partial melts that are magnesiocarbonatite in composition rather than calciocarbonatite (e.g., Wallace and Green, 1988; Dalton and Presnall, 1998; Klemme et al., 1995; Sweeney et al., 1995; Foley et al., 2009; Dasgupta et al., 2009). The key features of direct mantle-derived carbonatites were summarized by Bell and Rukhlov (2004), and include that these: 1- are dolomitic in nature with high Mg# and have few, if any, associated silicate rocks and high Mg# values; and 2- always contain some mantle minerals (Cr-rich minerals, diamond and/or graphite). Examples of carbonatite occurrences worldwide that are postulated to have been derived by direct partial melting of upper mantle include: Tamazert (Mourtada et al., 1997), Shawa and Dorowa (Harmer and Gittins, 1998), Newania (Doroshkevich et al., 2010), Spitskop (Harmer, 1999), Veseloe and Pogranichnoe (Doroshkevich et al., 2007a, 2007b), Wekusko Lake (Chakhmouradian et al., 2009), Snape Lake (Agashev et al., 2008) and Prairie Lake (Wu et al., 2016). The major element compositions for the dolomite analyzed here within the Blue River region (Table 1, Fig. 4) overlap those for worldwide occurrences (e.g., Spitskop), and are consistent with the compositions of the run products from melting experiments cited above; these in turn confirm their upper mantle derivation. Although the carbonate compositions for the samples investigated here define a bimodal distribution, their corresponding CN-REE patterns are similar and display LREE enrichment (Fig. 5), which is consistent with typical REE signatures of magmatic

Table 5
Pb isotope data for carbonate separates from the carbonatite samples.

Sample	U (ppm)	Pb (ppm)	Th (ppm)	$^{238}U/^{204}Pb$	$^{235}U/^{204}Pb$	$^{232}Th/^{204}Pb$	$^{206}Pb/^{204}Pb$	2σ	$^{207}Pb/^{204}Pb$	2σ	$^{208}Pb/^{204}Pb$	2σ
FIR-W	0.15	1.69	0.27	12.6	0.09	23.8	108.1	0.016	20.45	0.003	39.75	0.006
FIR-K	0.17	1.35	1.19	10.0	0.07	74.3	35.49	0.003	16.50	0.001	42.66	0.003
GUM	0.24	1.50	0.67	11.5	0.08	33.6	27.00	0.001	16.09	0.001	41.49	0.002
HW-CR	0.57	4.3	4.2	9.2	0.07	70.2	21.64	0.001	15.89	0.001	41.86	0.001
FLX	0.28	2.1	1.04	9.4	0.07	36.1	24.05	0.001	15.95	0.001	40.76	0.002
FEN-1	5.6	17	19	20.6	0.15	70.8	18.82	0.001	15.62	0.001	38.58	0.002
FEN-2	1.10	6.6	3.4	10.6	0.08	33.8	18.80	0.001	15.61	0.001	39.53	0.001
CHP-LK	0.18	0.62	1.3	19.9	0.14	148.7	24.80	0.001	16.02	0.001	40.60	0.002
JC-PR	0.12	0.23	0.52	34.8	0.25	150.2	19.97	0.001	15.64	0.001	39.52	0.001

Sample	$^{207}Pb/^{206}Pb$	2σ	$^{208}Pb/^{206}Pb$	2σ	$^{206}Pb/^{204}Pb(i)$	$^{207}Pb/^{204}Pb(i)$	$^{208}Pb/^{204}Pb(i)$
FIR-W	0.18920	0.00001	0.368	0.00002	107.4	20.42	39.34
FIR-K	0.46487	0.00001	1.202	0.00002	34.95	16.47	41.39
GUM	0.59585	0.00001	1.537	0.00002	26.38	16.06	40.92
HW-CR	0.73445	0.00001	1.935	0.00003	21.14	15.87	40.67
FLX	0.66323	0.00001	1.695	0.00003	23.30	15.91	39.86
FEN-1	0.83004	0.00001	2.049	0.00002	16.89	15.51	36.52
FEN-2	0.83045	0.00001	2.102	0.00002	17.81	15.56	38.55
CHP-LK	0.64613	0.00001	1.637	0.00002	21.38	15.77	32.88
JC-PR	0.78322	0.00001	1.979	0.00002	19.25	15.60	38.54

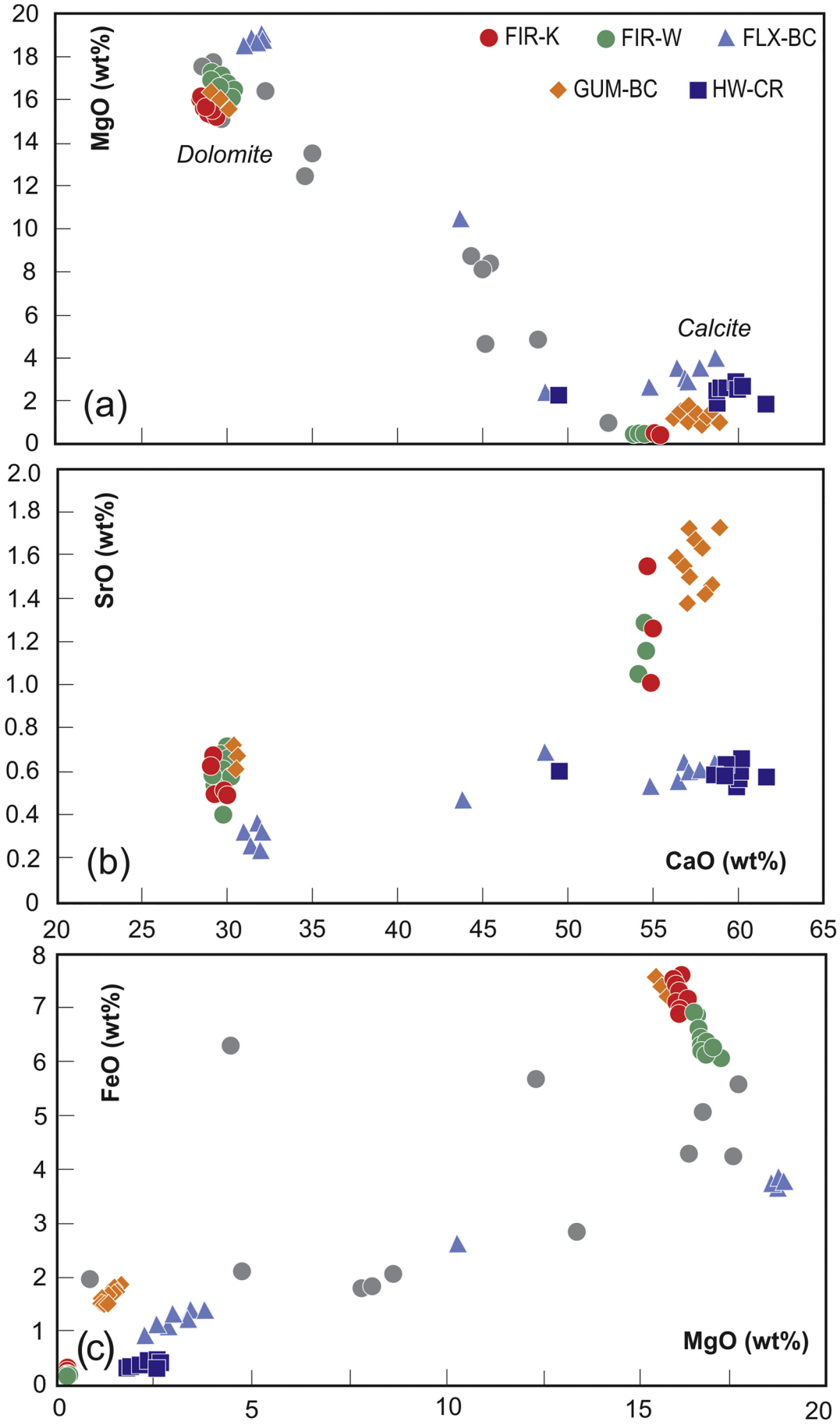

(caption on next page)

Fig. 4. Major and minor element compositions obtained by electron microprobe analyses for calcite and dolomite from carbonatite samples in the Blue River region. (a) MgO (wt%) and (b) SrO (wt%) vs. CaO (wt%), (c) FeO (wt%) vs MgO (wt%). Gray solid circles represent major element data from calcite carbonatite, dolomite–calcite carbonatite, dolomite carbonatite samples (whole rock) from the Spitskop Complex, South Africa (Harmer, 1999). (For interpretation of the references to colour in this figure legend, the reader is referred to the web version of this article.)

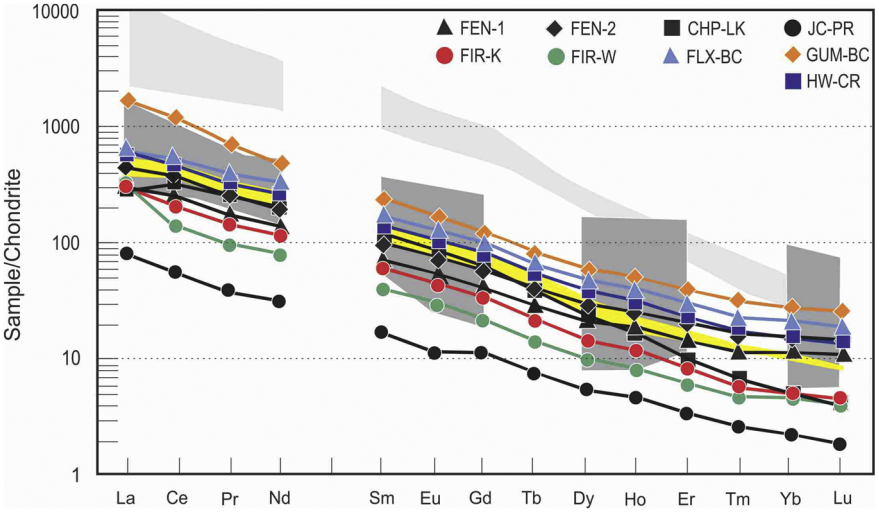

Fig. 5. Chondrite-normalized rare earth element patterns for carbonate separates from the carbonatite samples investigated here. Chondrite values are from McDonough and Sun (1995). Lighter gray field represents data for apatites from Blue River carbonatites (Mitchell et al., 2017), whereas darker gray field represents data for carbonatites (whole rock) from Spitskop Complex, South Africa (Harmer, 1999). Yellow field shows data from Fir dolomite carbonatites (Chudy, 2013). (For interpretation of the references to colour in this figure legend, the reader is referred to the web version of this article.)

carbonatites worldwide (e.g., Hornig-Kjarsgaard, 1998 and references therein). Moreover, the CN-REE patterns for the Blue River carbonatites overlap those for the dolomitic carbonatites from the Spitskop complex (Harmer, 1999; Fig. 5). The carbonate separates from both FIR samples, which are characterized predominantly by dolomite, contain the least TREE abundances among the Blue River carbonatites (Table 2; Fig. 5). Given the major element compositions described above, it is unlikely that the uniform CN-REE patterns for all samples investigated here are the result of closed-system melt differentiation from a single parental magma. A more plausible interpretation involves small degree partial melting of a heterogeneous (variably enriched) upper mantle source.

Of note, the CN-REE patterns from Chudy (2013) for the Fir dolomite carbonatites display similar patterns but plot at higher values compared to those determined here for carbonate separates from Fir (Fig. 5). One possible explanation for this difference is that the former are whole rock analyses and therefore may have incorporated REEs contributed by accessory minerals. Moreover, as documented in previous studies (e.g., Chen and Simonetti, 2013), the comparative results shown in Fig. 5 indicate that apatite controls the TREE budget over carbonate in carbonatite systems. The CN-REE patterns for carbonate from the Fir carbonatite ($TREE_{(CN)}$ = 85.5–113.4) are the least enriched compared to the remaining carbonatites from the Blue River region (e.g., Howard Creek, Felix and Gum; $TREE_{(CN)}$ = 250.3–590.9). This feature may be attributed to the predominantly dolomitic nature of the carbonate at Fir, which based on experimental results is characterized by lower partition coefficients for incompatible trace elements compared to calcite (e.g., Hornig-Kjarsgaard, 1998; Dasgupta et al., 2009). In addition, TREE abundances for Fen, Chipman Lake and Jacupiranga carbonatite samples are 423.5 ppm (average of two samples), 430 ppm and 80 ppm, respectively; the TREE content for the

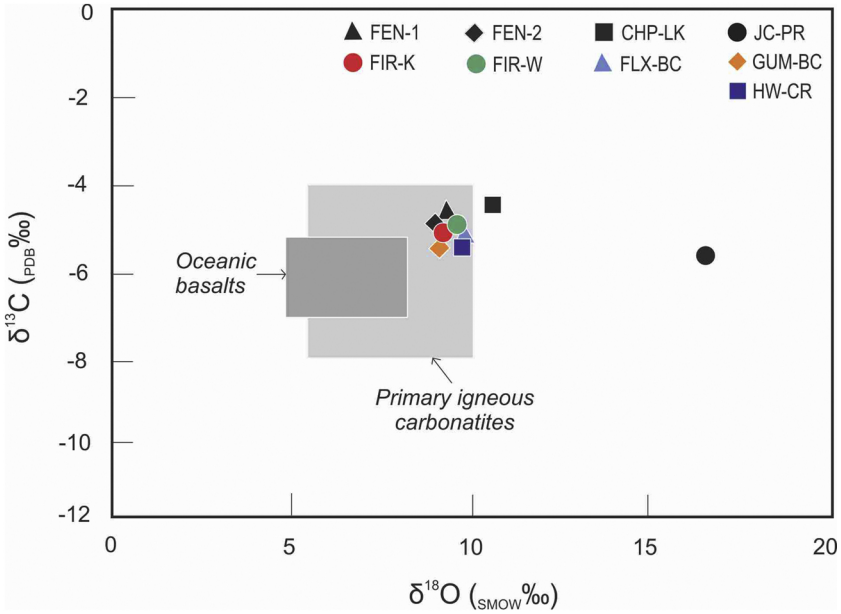

Fig. 6. Carbon and oxygen isotopic compositions for carbonate separates from the carbonatite samples investigated here. Primary igneous carbonatites (PIC) and oceanic basalts boxes are from Deines (1989) and Keller and Hoefs (1995), respectively.

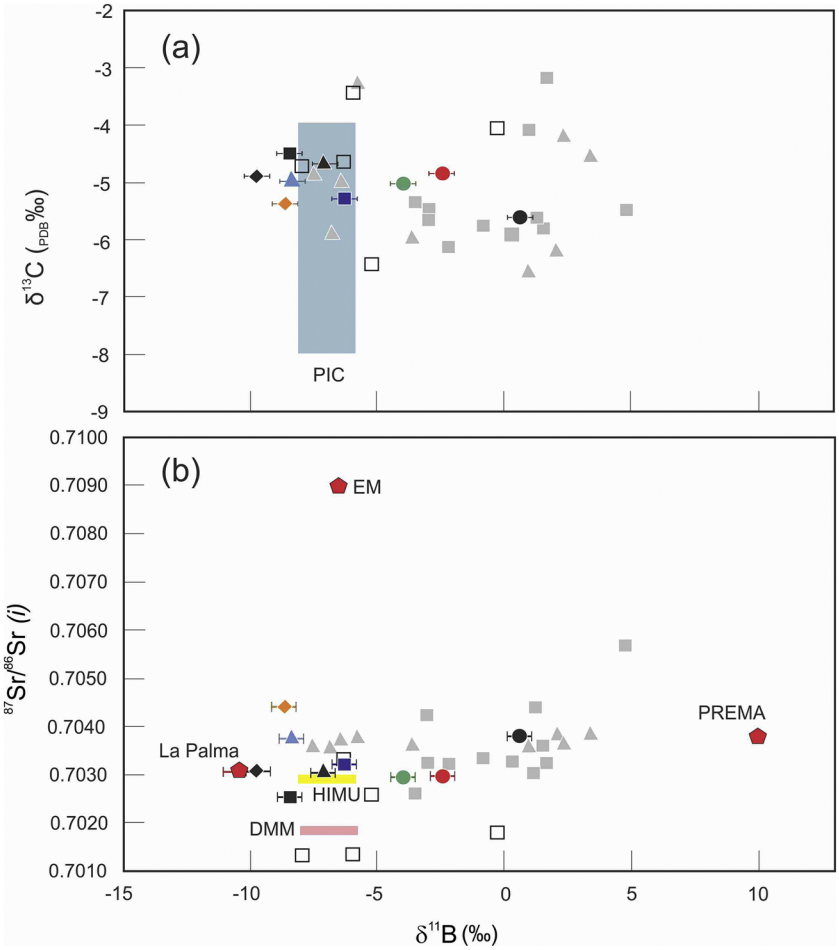

Fig. 7. Diagrams of $\delta^{13}C$ (a) and initial $^{87}Sr/^{86}Sr(i)$ (b) compositions vs $\delta^{11}B$ values for carbonate separates from the carbonatites investigated here. These are compared to those for carbonatite occurrences (gray square < 300 Ma; white square > 300 Ma) worldwide (Hulett et al., 2016) and Miaoya complex (gray triangle; Çimen et al., 2018). Sr isotope fields for HIMU and DMM are from Zindler and Hart (1986); note that asthenospheric $\delta^{11}B$ value of -7.1 ± 0.9‰ (Marschall et al., 2017) is attributed to these three mantle components. $\delta^{13}C$ values for PIC are from Deines (1989). Data for PREMA and EM ("DampEM") are from Dixon et al. (2017), and those for basalts from La Palma, Canary Islands are from Walowski et al. (2019). Symbols same as in Fig. 5.

Jacupiranga carbonate separate is particularly low compared to that for average carbonatite along with those of other trace elements reported here (e.g., Sr; Woolley and Kempe, 1989); its TREE content falls within the range defined for sedimentary carbonate (< 200 ppm; e.g., Xu et al., 2010 and references therein). Hence, these results for the Jacupiranga carbonate separate are rather suspect since they cannot be easily attributed to carbonatite melt derivation from partial melting of a metasomatized upper mantle source; however, its CN-REE pattern along with those for the Chipman Lake and Fen carbonate separates are similar to those for the carbonates from the Blue River area analyzed here (Fig. 5). The combined low TREE content and heavy $\delta^{18}O$ value of +16.55‰ suggests that the carbonate sample from Jacupiranga has been subjected to post-solidification alteration. Thus, this renders its radiogenic and B isotopic data suspect with regards to deciphering and evaluating the nature of its mantle source.

5.2. Nature of upper mantle source(s)

Oxygen and carbon stable isotope signatures of mantle-derived carbonates are effective in evaluating possible mantle sources, contamination or hydrothermal processes (e.g., Deines, 1989; Keller and Hoefs, 1995). All of the stable $\delta^{18}O$ and $\delta^{13}C$ isotope values reported here for the Blue River carbonatites (Table 3; Fig. 6) plot within the PIC field, which is indicative of their pristine nature and upper mantle origin. The sample from Chipman Lake plots marginally to the right of the PIC field, whereas the carbonate from Jacupiranga is characterized by a heavy O isotope signature (16.55‰; Fig. 6), and the latter may be attributed to low-temperature, sub-solidus alteration (e.g., Deines, 1989; Simonetti et al., 1995). Thus, with the exception of the carbonate sample from Jacupiranga, the remaining samples investigated here yield radiogenic and B isotopic data that can be used to decipher the nature of their upper mantle source(s).

In the recent study by Mitchell et al. (2017), apatite for several of these complexes (e.g., Howard Creek and Gum) clearly define a significant range in Sr isotope compositions that are not consistent with melt differentiation in a closed-system. Of particular interest is the fact that the carbonate (this study) and corresponding apatite from Blue River carbonatites yield similar or overlapping initial Sr isotope ratios (Mitchell et al., 2017), regardless of the tectonic deformation incurred by these samples. Moreover, Mitchell et al. (2017) proposed that the Sr and Nd isotopic compositions for apatites from the Blue River carbonatites were interpreted to suggest derivation from *depleted* sub-lithospheric mantle that is characterized by a mixed HIMU-EMI signature; however, it is somewhat contradictory to invoke the simultaneous occurrence of a long-lived "depleted" mantle that is characterized by HIMU and EMI signatures. The main reason being that the latter components are predominantly attributed to enriched, asthenospheric, plume-related mantle giving rise to oceanic island basalts (OIBs; e.g., Zindler and Hart, 1986).

The recent investigations of Hulett et al. (2016) and Çimen et al. (2018) have demonstrated that combining $\delta^{11}B$ isotope signatures with stable (C, O) and radiogenic (Nd, Pb, and Sr) isotope values for carbonatites is effective in providing additional insights with regards to their petrogenesis and nature of mantle source(s). For the Blue River carbonatites, the $\delta^{11}B$ isotope signatures for Gum, Howard Creek, and Felix either overlap or are very close to the range of values for typical asthenospheric (MORB) mantle (~ -7.1 ± 0.9‰; Marschall et al., 2017). In contrast, the $\delta^{11}B$ signatures for the Fir carbonatites (-3.98 and -2.47‰) are heavier and consistent with those for young (< 300 Ma old) carbonatites worldwide (Hulett et al., 2016; Fig. 7). Of

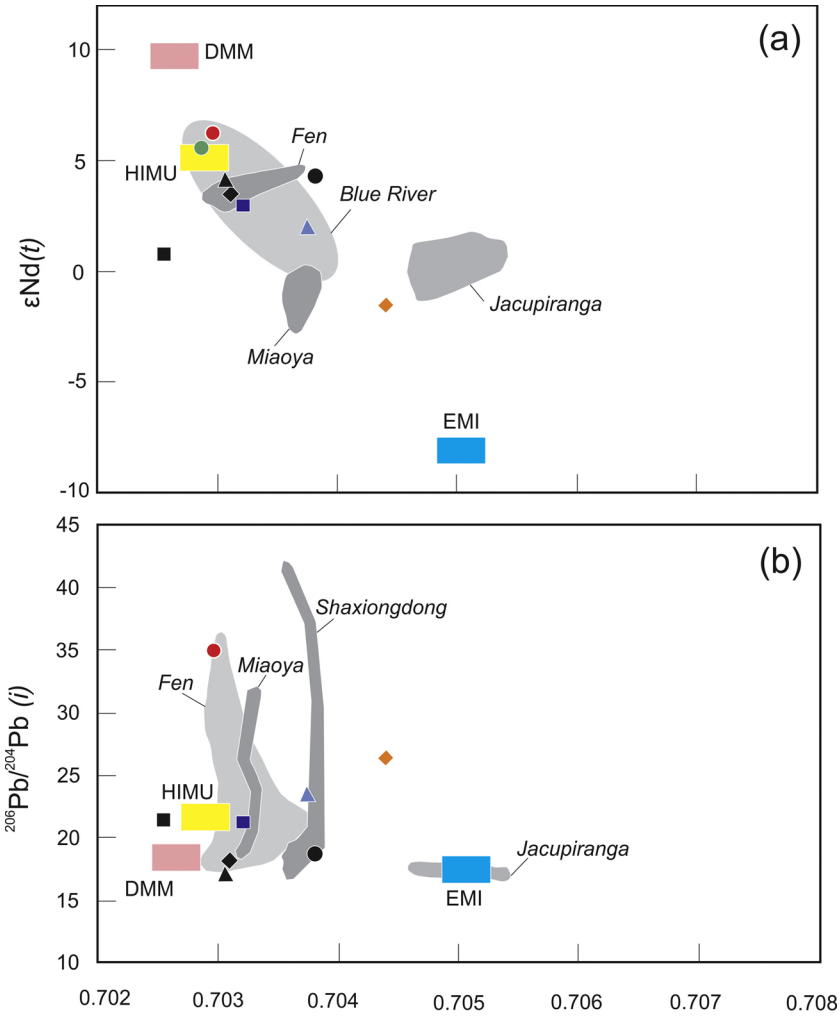

Fig. 8. Diagrams of initial $^{87}Sr/^{86}Sr(i)$ compositions vs ε_{Nd} (a) and $^{206}Pb/^{204}Pb(i)$ (b) values for carbonate separates from the carbonatites investigated here. HIMU, EMI and DMM fields are from Zindler and Hart (1986). Sources for the data are from the following previous studies: Blue River (Mitchell et al., 2017); Jacupiranga (Roden et al. 1985; Huang et al., 1995 and Beccaluva et al., 2017); Miaoya (Çimen et al., 2018); Shaxiongdong (Chen et al., 2018); Fen (Andersen, 1987). Results for FIR-W sample were excluded due to extremely radiogenic Pb isotope compositions (Table 5). Symbols same as in Fig. 5. (For interpretation of the references to colour in this figure legend, the reader is referred to the web version of this article.)

importance, the combined $\delta^{11}B$, $\delta^{13}C$, and $\delta^{18}O$ isotope signatures indicate that the carbonatites from Blue River region reflect those of their mantle source and are not the result of crustal contamination or subsolidus alteration processes (Fig. 7a). It has been well established that crustal assimilation will produce heavier $\delta^{18}O$ and $\delta^{13}C$ isotope compositions, which is clearly not the case here since all of the carbonates from the Blue River region plot within or proximal to the PIC field (Fig. 6). The initial $^{87}Sr/^{86}Sr$ isotope ratios for several of the Blue River carbonatites (e.g., Felix and Gum) display more radiogenic values relative to the remaining samples, and this suggests the presence of a heterogeneous mantle source involving more than one endmember. Here, the heavier $\delta^{11}B$ isotope values of −3.98‰ and − 2.47‰ (Table 3) for both carbonatite samples from Fir, which are greater than the range for typical asthenospheric mantle (~ −7.1 ± 0.9‰), may reflect input from recycled crustal material (Hulett et al., 2016). Overall, the $\delta^{11}B$, $\delta^{13}C$ and initial $^{87}Sr/^{86}Sr$ isotope signatures (Fig. 7) for the carbonatites investigated here are consistent with those for the Miaoya complex (Çimen et al., 2018) and carbonatite occurrences worldwide (Hulett et al., 2016). For the latter studies, the carbonatite complexes examined contained solely calcium carbonate and not dolomite. Here, both samples from Fir contain predominantly dolomite as their carbonate phase, and therefore, it is possible that their heavier $\delta^{11}B$ isotope signatures reflect melt-crystallization fractionation. However, the lack of anomalous or mixed B isotope values from these samples (i.e., intermediate values between an asthenospheric mantle and an endmember with heavier $\delta^{11}B$ isotope signature; Fig. 7) argues against this interpretation.

The Sr, Nd and Pb isotope systematics of young carbonatite occurrences (< 200 Ma old) worldwide suggest that these were derived from a heterogeneous mantle source including EMI and HIMU mantle components (Zindler and Hart, 1986; Bell and Simonetti, 2010). In Fig. 8a, the initial $^{87}Sr/^{86}Sr$ and $\varepsilon_{Nd(t)}$ values for the Blue River carbonatites, which indeed plot between the HIMU and EMI compositional fields, are also consistent with the involvement of these two mantle components during carbonatite melt generation; there is a lack of Nd, Pb and Sr isotopic evidence to suggest the involvement of depleted mantle (e.g., DMM- depleted MORB mantle; Fig. 8). Hence, the radiogenic isotope compositions corroborate the stable $\delta^{11}B$ isotope results, which indicate the presence of an enriched mantle source that contains recycled crustal material (Fig. 7b). Unlike the carbonatite worldwide occurrences investigated by Hulett et al. (2016), which all yielded mantle-like C and O isotope signatures (Fig. 7b), the heavy $\delta^{11}B$ value for the carbonate sample from Jacupiranga may be attributed to low-temperature alteration/hydrothermal processes given its extremely high $\delta^{18}O$ value of 16.55‰ (Table 3; Fig. 7b). Of particular note is the fact that the carbonate samples from Felix and Gum both contain asthenospheric-like $\delta^{11}B$ values of −8.38 and − 8.67‰, respectively regardless of their relatively radiogenic Nd and Sr isotope signatures compared to other Blue River carbonatites (Fig. 7b). This feature suggests that there may be more than one radiogenic mantle component present in the source of the Blue River carbonatites, and/or the B isotope signature for the EMI mantle component is not that of typical asthenospheric mantle as assumed and illustrated in Fig. 7b. If indeed the radiogenic isotope signatures of young carbonatites worldwide reflect mixing predominantly between HIMU and EMI mantle components (e.g., Bell and Simonetti, 2010), then one can perhaps infer that

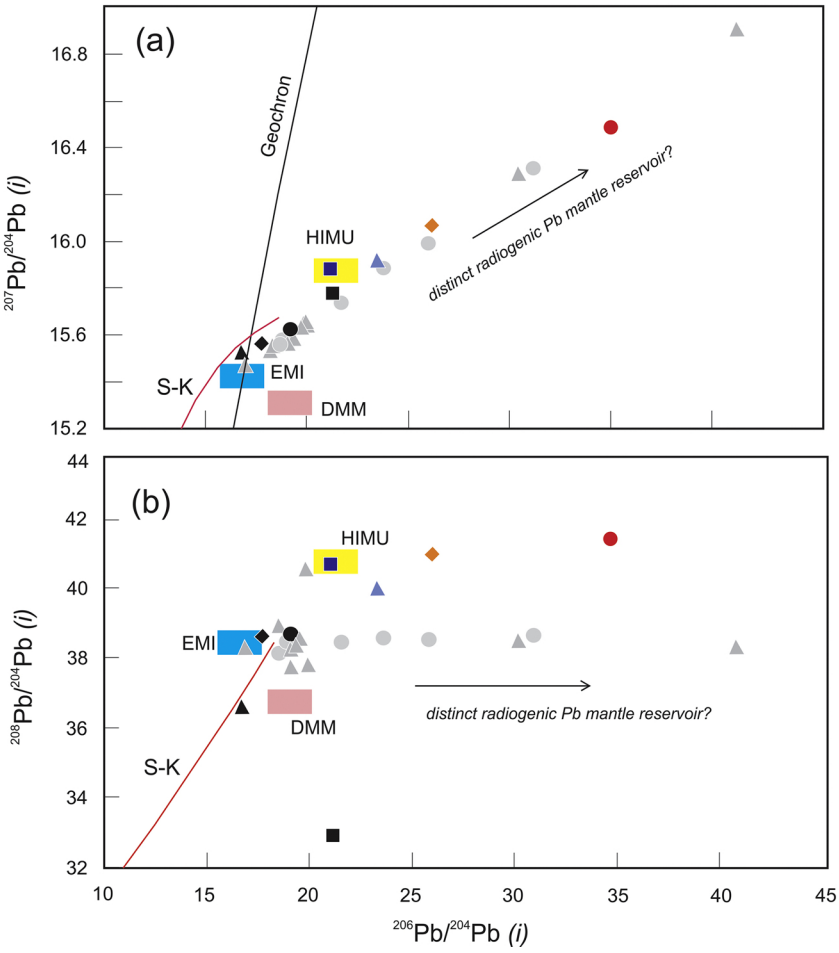

Fig. 9. Diagrams of initial $^{207}Pb/^{204}Pb(i)$ (a) and initial $^{208}Pb/^{204}Pb(i)$ (b) compositions vs $^{206}Pb/^{204}Pb(i)$ values for carbonate separates from the carbonatites investigated here. These are compared to those for carbonatite occurrences from South Qinling, China (gray triangle: Miaoya complex, Çimen et al., 2018; gray circle: Shaxiongdong carbonatite, Chen et al., 2018). HIMU, EMI and DMM fields are from Zindler and Hart (1986). The 4.56 Ga Geochron is also plotted in A. S-K: Stacey-Kramers 2-stage Pb evolution curve (Stacey and Kramers, 1975). Results for FIR-W sample were excluded due to extremely radiogenic Pb isotope compositions (Table 5). Symbols same as in Fig. 5.

the $\delta^{11}B$ value for EMI is not the typical asthenospheric value of -7.1 ± 0.9‰ (Marschall et al., 2017) based on the distribution of the Sr and B isotope data (Fig. 7b).

It is somewhat difficult to directly compare commonly used geochemical tracers (e.g., B/Zr, B/Nb) adopted for delineating mantle processes and source characteristics for primitive, mafic basalts to those measured in carbonatites due to contrasting magma types (silicate- vs. carbonate-dominated) and consequently distinct melt differentiation processes. Moreover, it has been clearly established that a majority of carbonatites worldwide do not represent primitive liquid compositions but rather are cumulate in nature (e.g., Mitchell, 2005). In addition, previous investigations have demonstrated that the stable, light isotope compositions of oceanic island basalts (OIBs), such as $\delta^{7}Li$ and $\delta^{11}B$, must be carefully screened and evaluated for shallow level crustal contamination (e.g., assimilation-fractional crystallization; Genske et al., 2014). Nonetheless, comparison of the $\delta^{11}B$ and radiogenic Nd, Pb, and Sr isotope signatures between carbonatites and those for (unaltered and uncontaminated) MORBs, and in particular enriched-MORBs and OIBs, may shed some important insights into the chemical nature of mantle source(s) for the former. For example, Dixon et al. (2017) report abundances of volatiles (CO_2, H_2O, Cl), δD_{SMOW} values, and new $\delta^{11}B$ compositions for enriched basalts from various mid-ocean ridge segments from both Pacific and Atlantic Oceans. Basalts from the Shona (Group I) in the southern mid-Atlantic ridge segment, which are characterized by PREMA (Prevalent Mantle) Pb and Sr isotope signatures, yield heavy $\delta^{11}B$ values of +10‰ (Fig. 7). The latter may be attributed to the generation of isotopically enriched boron from antigorite within the deep mantle (Benton et al., 2001; Spivack and Edmond, 1987). In addition, Dixon et al.'s (2017) "DampEM" or Enriched Mantle (EM) component based on C-O-H-Cl fluid compositions is characterized by $^{87}Sr/^{86}Sr$ and $\delta^{11}B$ values of 0.709 and − 6.6‰, respectively and this component is also shown in Fig. 7b. The B isotope signature of the DampEM component is consistent with that of dehydrated sediments (−1 to −8‰; Ishikawa and Nakamura, 1993), or melange serpentinites resulting from mantle wedge hydration at significant depths (30 to > 70 km; Martin et al., 2016). Dixon et al. (2017) proposed a multistage dehydration model to account for the contrasting isotopic compositions, which takes into account the thermal properties of the subducting slab. This in turns provides an important control on the concentrations of volatiles and light stable isotopic composition of slab materials. Hence, it was proposed that EM-like mantle results from the melting of carbonated sediments of a subducting slab at roughly 230 km depth, whereas a PREMA-like mantle reservoir is located deeper (> 300 km) and produced by slab interaction with fluids derived from dehydrated subcrustal antigorite (Dixon et al., 2017).

The recent study of Walowski et al. (2019) investigated the B and volatile (H_2O, CO_2, and Cl) abundances and $\delta^{11}B$ compositions of basaltic glasses and olivine-hosted melt inclusions from OIBs present at La Palma, Canary Islands, and Piton de Caille, La Réunion Island. The olivine-hosted melt inclusions provide more robust estimates of primary mantle source $\delta^{11}B$ values compared to previous studies investigating whole rocks since the former are protected from contamination during ascent. The average $\delta^{11}B$ value for the La Réunion samples (-7.9 ± 0.5‰; 2σ) overlaps that for MORB, whereas basalts from La Palma, which are notable for their radiogenic Pb isotope ratios, contain distinctly lighter $\delta^{11}B$ values of -10.5 ± 0.7 (2σ) (Walowski et al., 2019; Fig. 7). Walowski et al. (2019) suggest that the isotopically light $\delta^{11}B$ values are derived from considerably dehydrated recycled materials, which is consistent with their B/Zr and H_2O/Ce ratios. Thus, upon examination of the data illustrated in Fig. 7b, it is clear that the new B

isotope compositions reported here for the Blue River carbonatites along with those measured to date for carbonatite occurrences worldwide plot within a field/area bounded by MORB (typical asthenospheric mantle), PREMA-, DampEM (or enriched mantle, EM)-, and a mantle source similar to the one giving rise to the OIBs in La Palma (Canary Islands). Thus, several straightforward interpretations are possible: 1- recycled crustal materials of varying B isotopic compositions are playing an important role in the mantle source regions of carbonatite melt generation; and 2- carbonatites are tapping similar mantle sources that are giving rise to MORBs and OIBs worldwide; this is consistent with the similar Nd-Sr-Pb isotope systematics between OIBs and carbonatites (see Bell and Simonetti, 2010 for detailed review).

The extremely radiogenic Pb isotope ratios for the Blue River carbonatites (e.g. Fir carbonatite) may indicate involvement of a distinct radiogenic Pb mantle reservoir (Figs.8b and 9). The similar distributions in radiogenic Pb isotope values for the Miaoya (Çimen et al., 2018), Shaxiongdong (Chen et al., 2018) and Fen (Andersen, 1987) carbonatite complexes all corroborate the involvement of a distinct, radiogenic Pb mantle reservoir for carbonatite melt generation (Fig. 8b). Of note, the Pb isotope values from the Miaoya and Shaxiongdong complexes display a wide range of values, whereas their corresponding $^{87}Sr/^{86}Sr$ signatures define narrow ranges (0.70357–0.70384 and 0.70319–0.70331, respectively). Chen et al. (2018) previously suggested that the chemical and Pb isotopic compositions of carbonatites from the Shaxiongdong region (China) indicate involvement of a distinct, highly radiogenic Pb mantle reservoir. A similar type of mantle reservoir is needed to explain the extremely radiogenic Pb isotope data for a majority of the carbonates from both the Blue River region and Fen samples investigated here since these plot to the right of HIMU (Table 5; Figs. 8b and 9); this result suggests that the presence of an extremely radiogenic Pb isotope reservoir may be a more prevalent global phenomenon than previously postulated. In contrast, the Jacupiranga carbonatites define a narrow range in terms of radiogenic Pb isotope ratios and this complex could have been generated from mixing of HIMU and EMI mantle sources (Fig. 8b).

In summary, the combined isotopic signatures reported in this study provide significant information about the heterogeneous character of the upper mantle beneath this region of the North American craton, and requires the involvement of several mantle components including HIMU, PREMA, EM-like, and a distinct radiogenic Pb reservoir (Figs. 8 and 9). In previous studies, it has been argued that these enriched mantle reservoirs are typically associated with plume-related magmatism (e.g., Gasperini et al., 2000; Bell et al., 2006; Bell and Simonetti, 2010); however, this interpretation is difficult to argue here given their emplacement within a local, extensional environment in a subduction-related tectonic regime.

5.3. Tectonic context: subduction zones vs rift environments?

Carbonatites generally occur within stable, intra-plate, continental regions and continental rifts, and rarely in orogenic belts or within oceanic plates (e.g., Nelson et al., 1988; Woolley and Kjarsgaard, 2008. The vast majority of previous investigations of carbonatite complexes have focused on those from anorogenic tectonic environments and not those found within collision/subduction zone-related carbonatite complexes (e.g., Hou et al., 2006; Chen et al., 2018; Çimen et al., 2018). Within anorogenic regimes, carbonatite melts may be related to mantle plume activity and linked to a volatile-rich, isotopically heteregeneous asthenospheric/plume source (e.g., Bell and Simonetti, 2010).

Numerous previous studies have well established that the boron budget and $\delta^{11}B$ signatures of arc-related magmatism are controlled by subduction-related processes (e.g., Leeman et al., 2017). However, it remains unclear whether recycling involves bulk mixing of subducted material into arc magma sources, or selective transfer via devolatilization fluids, partial melts, or both (e.g., Class et al., 2000; Elliott et al., 1997; Klimm et al., 2008; Plank, 2005). Within active subduction zones, it has been suggested that carbonatitic melts are derived from the metasomatised lithospheric mantle that was modified by infiltration of high-flux REE- and CO_2-rich fluids derived from subducted marine sediments (e.g., D'Orazio et al., 2007; Bonadiman et al., 2008; Deng et al., 2014; Hou et al., 2006, 2015). Similarly, the recent study by Li et al. (2019) reports new Mo isotope compositions, along with B isotopic and trace element data for a suite of Cenozoic basalts from the eastern North China Craton (NCC). The combined isotopic and geochemical results suggest that the nephelinites and basanites were derived from a carbonated mantle source via fluid-flux melting (Li et al., 2019). The origin of the fluid flux is somewhat complex within an intraplate setting; however, it could be associated to the decarbonization of subducted slabs stalled in the deep mantle. The interaction between these ascending carbonate-rich fluids (from depths of 300 km or more) and an extensive column of depleted mantle will modify and alter their original B isotopic composition to that of depleted upper mantle (Li et al., 2019).

The Blue River region contains an important series of carbonatite complexes associated with a collision-type tectonic setting (Fig. 1), postulated to have formed during the rifting and extensional episodes in the Late Cambrian and Devono-Mississippian times (e.g., Gorham et al., 2009; Millonig et al., 2012). Based on recently published geochronological data (Millonig et al., 2012), the magmatism in the southern Canadian Cordillera formed discontinuously during the Neoproterozoic, Late Cambrian and Upper Devonian to Lower Carboniferous. Most of the carbonatite samples (e.g., Fir, Gum, Howard Creek) from the Blue River region investigated here were emplaced in the Devono-Mississippian, whereas the Felix carbonatite intruded in the Late Cambrian. As stated above, the stable (Figs. 6 and 7) and radiogenic isotope (Figs. 8 and 9) signatures for the Blue River carbonatites indicate derivation from a heteregenous mantle source that may include HIMU, PREMA, EM-like, components and a distinct radiogenic Pb reservoir. Rukhlov et al. (2018b) report Sr, Nd, and Pb isotope data for the same carbonatites from the Blue River area investigated here, and these define a mixing trend involving FOZO (Focal Zone) and EMI mantle end-members. Although HIMU, EMI, and FOZO mantle component signatures recorded by young (< 200 Ma) carbonatites are typically associated with OIBs and mantle plume activity (e.g., Bell and Simonetti, 2010), it is doubtful that the Blue River region carbonatites are the products of plume activity as there are no physical and petrological evidences for the latter impacting the area of study; i.e., regional crustal doming, presence of extensive flood basaltic province, and radial dyke swarms (e.g., Sleep, 1990; Davies, 1999; Rainbird and Ernst, 2001; Saunders et al., 2007). Alternatively, it is more likely that enriched fluids/melts were tapped from the underlying, convecting (isotopically enriched) asthenosphere during periods of extension, which may have caused decompression melting of the asthenosphere with ascending partial melts metasomatizing the overlying lithosphere (e.g., Bell and Simonetti, 2010).

In contrast, the Cambrian-aged Fen carbonatite, which is located west of the Oslo rift, is a well known example of carbonatite magmatism associated with extensional rifting in an anorogenic tectonic setting (e.g., Andersen and Taylor, 1988). It is characterized by negative $\delta^{11}B$ isotope values (−7.12 and − 9.79‰) (Fig. 7), which is consistent with the B isotope results of carbonatite occurrences worldwide for complexes older than ~300 Ma since these are characterized by asthenopheric-like values (−7.1 ± 0.9‰; Hulett et al., 2016; Marschall et al., 2017). Based on Nd, Pb, and Sr isotope compositions (Fig. 8), the carbonatites from Fen display signatures that are indicative of derivation from a mixed mantle source region consisting of enriched mantle components (e.g., HIMU, EMI and distinct radiogenic Pb reservoir). In contrast, sample JC-PR from the younger, early Cretaceous Jacupiranga carbonatite yields a $\delta^{11}B$ isotope value (0.62‰) that is more positive than the remaining older carbonatites investigated here (Table 3 and Fig. 7). However, its elevated $\delta^{18}O$ value of 16.55‰ (Table 3) renders

this B isotope result suspect and precludes it from providing meaningful information in relation to the chemical nature of its mantle source. The combined O and B isotope ratios for JC-PR suggest this sample has most likely undergone subsolidus alteration/contamination, which may also explain its somewhat odd Nd and Sr isotope signatures (Fig. 8) relative to the other samples examined here. Moreover, sample JC-PR is also characterized by extremely low concentrations of incompatible elements such as Sr and the REEs (Table 2) compared to other samples investigated here, and those characteristic of average pristine, 'fresh' mantle-derived carbonatites (e.g., Woolley and Kempe, 1989). Finally, sample CHP-LK from the Chipman Lake carbonatite is the oldest sample (1022 ± 31 Ma; Sage, 1985) and, yields a negative $\delta^{11}B$ isotope value of −8.48‰ combined with mantle-like $\delta^{13}C$ and $\delta^{18}O$ signatures (Table 3) and CN-REE patterns that are typical of mantle-derived carbonatites (Fig. 5). Thus, the combined compositional and isotopic evidence indicates that sample CHP-LK represents pristine/unaltered carbonatite, with the radiogenic (Nd, Pb, and Sr) and B isotope values indicating contrasting mantle sources. The former indicate derivation from an enriched upper mantle source compared to radiogenic signatures for carbonatites worldwide of similar age (Bell and Simonetti, 2010), whereas the B isotope data suggests derivation from typical asthenospheric mantle. However, the B isotope value of −8.48‰ for sample CHP-LK is consistent with the findings from Hulett et al. (2016), which argue that carbonatites older than 300 million years did not sample or incorporate recycled crustal material within their mantle source region.

Although the carbonatites within the Blue River area are generally sheared and recrystallized as a result of tectonism, on the basis of data reported in this study, it is clear that these have not been perturbed and have retained their original signatures inherited from their mantle source. The thicker (larger) dolomitic carbonatites such as Fir, are typically coarse-grained and are characterized by gneissic texture indicative of equilibration during metamorphism (Chudy, 2013). In addition, the calcite-dolomite geothermometry results obtained by Chudy (2013) using the least deformed carbonatite samples from the Blue River area yield temperatures ~50 °C higher than those of the local, regionally metamorphosed dolomitic marbles (630–650 °C). Hence, these results were interpreted to indicate magmatic crystallization conditions for the Fir carbonatites (Chudy, 2013). Therefore, this study is the first to report preservation of mantle-like $\delta^{11}B$ isotope signatures in metamorphosed and deformed carbonatites, which further confirms its great utility as a tracer of magmatic processes within crustal regimes. Moreover, the more positive $\delta^{11}B$ isotope values for the carbonates from Fir clearly confirm the presence of recycled crustal material within their mantle source.

6. Conclusions

The major, minor and trace element compositions of magmatic carbonates from the Blue River carbonatites (British Columbia, Canada) investigated here most probably reflect those inherited from their mantle source, and have not been perturbed by the complex tectono-metamorphic history of the region. The major element compositions of the dolomitic carbonates are consistent with those experimentally determined by direct partial melting of a metasomatized peridotite upper mantle source. Moreover, the combined compositional and mantle-like (B, C, O, Nd, Pb, and Sr) isotopic data for all of the calcitic and dolomitic carbonates reported in this study cannot be reconciled with melt differentiation involving closed system, fractional crystallization of a single parental melt. Their upper mantle source is chemically heterogeneous, and is characterized by the presence of HIMU and EM-like mantle components and a highly radiogenic Pb isotope endmember. The carbonatite complexes investigated here occur within a collisional-type tectonic environment, but were emplaced during extensional regimes within several orogenic cycles; in particular, the complexes younger than 360 Ma most likely formed due to extension caused by slab rollback. The first reported B isotope signatures for the carbonates from the Blue River region are not anomalous when compared to signatures for modern-day mid-ocean ridge basalts (MORBs) and oceanic island basalts (OIBs). Most are characterized by asthenosphere-like values with the exception of the carbonate from Fir. The latter contains slightly more positive $\delta^{11}B$ values that are consistent with those from young (< 300 Ma) carbonatite complexes worldwide, and corroborate the presence of recycled crustal carbon within its mantle source. Finally, the pristine, mantle-like $\delta^{11}B$ values for the Blue River carbonatites clearly demonstrate that this isotope system is robust and was not perturbed by the later tectono-metamorphic events. This observation indicates that B isotope signatures can be a valuable forensic tool for deciphering the nature of sources of mantle-derived carbonates.

Acknowledgements

We thank Drs. Dana Biasatti (CEST) and Ian Steele for assistance with O and C isotope and EPMA analyses, respectively. This research was in part financially supported by the University of Notre Dame. The first author also thanks The Scientific and Technological Research Council of Turkey (BIDEB-2219 programme) for providing a post-doctoral stipend. We also appreciate the comments provided by Drs. Catherine Chauvel, and Leo J. Millonig and an anonymous reviewer, which have resulted in an improved manuscript.

Appendix A. Supplementary data

Supplementary data associated with this article can be found, in the online version, at doi:10.1016/j.chemgeo.2019.07.015.

References

Agashev, A.M., Pokhilenko, N.P., Takazawa, E., McDonald, J.A., Vavilov, M.A., 2008. Primary melting sequence of a deep (> 250 km) lithospheric mantle as recorded in the geochemistry of kimberlite–carbonatite assemblages, Snap Lake dyke system, Canada. Chem. Geol. 255 (3), 317–328.
Amaral, G., 1978. Potassium-argon age studies on the Jacupiranga alkaline district, State of São Paulo, Brazil. Proceedings of the 1st Int. Symposium on Carbonatites, Poços de Caldas, Brazil 297–302.
Andersen, T., 1987. Mantle and crustal components in a carbonatite complex, and the evolution of carbonatite magma: REE and isotopic evidence from the Fen complex, S.E. Norway. Chem. Geol. Isotope Geosci. Sect. 65, 147–166.
Andersen, T., Taylor, P.N., 1988. Pb isotope geochemistry of the Fen carbonatite complex, S.E. Norway: Age and petrogenetic implications. Geochim. Cosmochim. Acta 52, 209–215.
Beccaluva, L., Bianchini, G., Claudio, N., Siena, F., 2017. The alkaline-carbonatite complex of Jacupiranga (Brazil): Magma genesis and mode of emplacement. Gondwana Res. 44, 157–177.
Bell, K., Blenkinsop, J., 1987. Archean depleted mantle-evidence from Nd and Sr initial isotope ratios of carbonatites. Geochim. Cosmochim. Acta 51, 291–298.
Bell, K., Rukhlov, A.S., 2004. Carbonatites from the Kola Alkaline Province: Origin, evolution and source characteristics. In: In: Zaitsev, A., Wall, F. (Eds.), Phoscorites and Carbonatites from Mantle to Mine: The Key Example of the Kola Alkaline Province: London Miner Soc Series, vol. 10. pp. 421–455.
Bell, K., Simonetti, A., 1996. Carbonatite magmatism and plume activity: implications from the Nd, Pb and Sr isotope systematics of Oldoinyo Lengai. J. Petrol. 37, 1321–1339.
Bell, K., Simonetti, A., 2010. Source of parental melts to carbonatites–critical isotopic constraints. Miner. Petrol. 98, 77–89.
Bell, K., Tilton, G.R., 2002. Probing the mantle: the story from carbonatites. EOS, American Geophysical Union 83 (25), 273–277.
Bell, K., Blenkinsop, J., Cole, T.J.S., Menagh, D.P., 1982. Evidence from Sr isotopes for long-lived heterogeneities in the upper mantle. Nature 298, 251–253.
Bell, K., Castorina, F., Rosatelli, G., Stoppa, F., 2006. Plume activity, magmatism, and the geodynamic evolution of the Central Mediterranean. Ann. Geophys-Italy 49, 357–371.
Benton, L.D., Ryan, J.G., Tera, F., 2001. Boron isotope systematics of slab fluids as inferred from a serpentine seamount, Mariana forearc. Earth Planet. Sci. Lett. 187, 273–282.
Bonadiman, C., Coltorti, M., Duggen, S., Paludetti, L., Siena, F., Thirwall, M.F., Upton, B.G.J., 2008. Palaeozoic subduction-related and kimberlite or carbonatite metasomatism in the Scottish lithospheric mantle. Geol. Soc. Spec. Publ. 293, 303–333.
Buckley, H.A., Woolley, A.R., 1990. Carbonates of the magnesite-siderite series from four carbonatite complexes. Mineral. Mag. 54, 413–418.
Chakhmouradian, A., Böhm, C.O., Demény, A., Reguir, E., Hegner, E., Creaser, R.A., Halden, N.M., Yang, P., 2009. "Kimberlite" from Wekusko Lake, Manitoba: actually a

diamond-indicator-bearing dolomite carbonatite. Lithos 112, 347–357.
Chaussidon, M., Jambon, A., 1994. Boron content and isotopic composition of oceanic basalts: geochemical and cosmochemical implications. Earth Planet. Sci. Lett. 259, 541–556.
Chen, W., Simonetti, A., 2013. In-situ determination of major and trace elements in calcite and apatite, and U–Pb ages of apatite from the Oka carbonatite complex: Insights into a complex crystallization history. Chem. Geol. 353, 151–172.
Chen, W., Lu, J., Jiang, S.Y., Ying, Y.C., Liu, Y.S., 2018. Radiogenic Pb reservoir contributes to the rare earth element (REE) enrichment in South Qinling carbonatites. Chem. Geol. 494, 80–95.
Chudy, T.C., 2013. The Petrogenesis of the ta-Bearing fir Carbonatite System, East-Central British Columbia, Canada. PhD Thesis. The University of British Columbia (553 p).
Çimen, O., Kuebler, C., Monaco, B., Simonetti, S.S., Corcoran, L., Chen, W., Simonetti, A., 2018. Boron, Carbon, Oxygen and Radiogenic Isotope Investigation of Carbonatite from the Miaoya complex, central China: Evidences for late-stage REE hydrothermal event and mantle source heterogeneity. Lithos 322, 225–237.
Class, C., Miller, D.M., Goldstein, S.L., Langmuir, C.H., 2000. Distinguishing melt and fluid subduction components in Umnak volcanics. Aleutian arc. Geochem. Geophys. Geosyst. 1 (6), 1004.
Costanzo, A., Moore, K.R., Wall, F., Feely, M., 2006. Fluid inclusions in apatite from Jacupiranga calcite carbonatites: evidence for a fluid-stratified carbonatite magma chamber. Lithos 91, 208–228.
Dahlgren, S., 1994. Late Proterozoic and Carboniferous ultramafic magmatism of carbonatitic affinity in southern Norway. Lithos 31, 141–154.
Dalton, J.A., Presnall, D.C., 1998. The Continuum of primary carbonatitic– kimberlitic melt compositions in equilibrium with lherzolite: data from the system CaO–MgO–Al2O3–SiO2–CO2 at 6 GPa. J. Petrol. 39 (11 − 12), 1953–1964.
Dasgupta, R., Hirschmann, M.M., McDonough, W.F., Spiegelman, M., Withers, A.C., 2009. Trace element partitioning between garnet lherzolite and carbonatite at 6.6 and 8.6 GPa with applications to the geochemistry of the mantle and of mantle-derived melts. Chem. Geol. 262, 57–77.
Davies, G.F., 1999. Dynamic Earth: Plates, Plumes and Mantle Convection. Cambridge University Press, U.K, pp. 458.
Deines, P., 1989. Stable Isotope Variations in Carbonatites: Carbonatites: Genesis and Evolution. Unwin Hyman vol. 13.
Deng, L.L., Liu, Y., Gao, S., 2014. Pacific slab subduction-induced carbonatite mantle metasomatism in the eastern North China Craton. In: Fall Meeting, Abstract #V. American Geophysical Union. pp. 13B–4774.
Dixon, J.E., Bindeman, I.N., Kingsley, R.H., Simons, K.K., Le Roux, P.J., Hajewski, T.R., Swart, P., Langmuir, C.H., Ryan, J.G., Walowski, K.J., Wada, I., Wallace, P.J., 2017. Light Stable Isotopic Compositions of Enriched Mantle sources: Resolving the Dehydration Paradox. Geochem. Geophy. Geosy. 18 (11), 3801–3839.
D'Orazio, M., Innocenti, F., Tonarini, S., Doglioni, C., 2007. Carbonatites in a subduction system: the Pleistocene alvikites from Mt. Vulture (southern Italy). Lithos 98, 313–334.
Doroshkevich, A.G., Wall, F., Ripp, G.S., 2007a. Magmatic graphite in dolomite carbonatite at Pogranichnoe, North Transbaikalia, Russia. Contrib. Mineral. Petrol. 153, 339–353.
Doroshkevich, A.G., Wall, F., Ripp, G.S., 2007b. Calcite-bearing dolomite carbonatite dykes from Veseloe, North Transbaikalia, Russia and possible Cr-rich mantle xenoliths. Mineral. Petrol. 90, 19–49.
Doroshkevich, A.G., Ripp, G., Viladgar, S., 2010. Newania carbonatites, Western India: example of mantle derived magnesium carbonatites. Miner. Petrol. 98 (1–4), 283–295.
Elliott, T., Plank, T., Zindler, A., White, W.M., Bourdon, B., 1997. Element transport from subducted slab to juvenile crust at the Mariana Arc. J. Geophys. Res. 102, 14,991–15,019.
Ernst, R.E., Bell, K., 2010. Large igneous provinces (LIPs) and carbonatites. Miner. Petrol. 98, 55–76.
Foley, S.F., Yaxley, G.M., Rosenthal, A., Buhre, S., Kiseeva, E.S., Rapp, R.P., Jacop, D.E., 2009. The composition of near-solidus melts of peridotite in the presence of CO_2 and H_2O between 40 and 60 kbar. Lithos 112 (1), 274–283.
Gasperini, D., Blichert-Toft, J., Bosch, D.C., Del Moro, A., Macera, P., Télouk, P., Albarède, F., 2000. Evidence from Sardinian basalt geochemistry for recycling of plume heads into the Earth's mantle. Nature 408, 701–704.
Genske, F.S., Turner, S.P., Beier, C., Chu, M.F., Tonarini, S., Pearson, N.J., Haase, K.M., 2014. Lithium and boron isotope systematics in lavas from the Azores islands reveal crustal assimilation. Chem. Geol. 373, 27–36.
Gorham, J., Ulry, B., Brown, J., 2009. 2008 Diamond Drilling and Exploration at the Blue River Property, B.C. Technical Report. B.C. Minister of Energy, Mines and Petroleum Resources.
Hall, C.E., Cooper, A.F., Parkinson, D.L., 1995. Early Cambrian carbonatite in Antarctica. J. Geol. Soc. Lond. 152, 721–728.
Harmer, R.E., 1999. The petrogenetic association of carbonatite and alkaline magmatism: constraints from the spitskop complex, South Africa. J. Petrol. 40 (4), 525–548.
Harmer, R.E., Gittins, J., 1998. The case for primary, mantle-derived carbonatite magma. J. Petrol. 39 (11–12), 1895–1903.
Hoernle, K., Tilton, G., Le Bas, M.J., Duggen, S., Garbe-Schönberg, D., 2002. Geochemistry of oceanic carbonatites compared with continental carbonatites; mantle recycling of oceanic crustal carbonate. Contrib. Mineral. Petrol. 142, 520–542.
Hornig-Kjarsgaard, I., 1998. Rare earth elements in Sövitic carbonatites and their mineral phases. J. Petrol. 39 (11–12), 2105–2121.
Hou, Z., Liu, Y., Tian, S., Yang, Z., Xie, Y., 2015. Formation of carbonatite-related giant rare-earth-element deposits by the recycling of marine sediments. Sci. Rep. 5 (10231), 1–10.
Hou, Z.Q., Tian, S., Yuan, Z., Xie, Y., Yin, S., Yi, L., Fei, H., Yang, Z., 2006. The Himalayan collision zone carbonatites in western Sichuan, SW China: Petrogenesis, mantle source and tectonic implication. Earth Planet. Sci. Lett. 244, 234–250.
Huang, J.M., Hawkesworth, C.J., van Calsteren, P.W.C., McDermott, F., 1995. Geochemical characteristics and origin of the Jacupiranga carbonatites, Brazil. Chem. Geol. 119, 79–99.
Hulett, S.R.W., Simonetti, A., Rasbury, E.T., Hemming, N.G., 2016. Recycling of subducted crustal components into carbonatite melts revealed by boron isotopes. Nat. Geosci. 9, 904–908.
Ishikawa, T., Nakamura, E., 1993. Boron-isotope systematics of marine sediments. Earth Planet. Sci. Lett. 117, 567–580.
Jones, A.P., Genge, M., Carmody, L., 2013. Carbonate melts and carbonatites. Rev. Mineral. Geochem. 75, 289–322.
Keller, J., Hoefs, J., 1995. Stable Isotope Characteristics of recent Natrocarbonatites from Oldoinyo Lengai. Carbonatite Volcanism. IAVCEI Proceedings in Volcanology, vol. 4, 113–123.
Klemme, S., van der Lan, S.R., Foley, S.F., Günther, D., 1995. Experimentally determined trace and minor element partitioning between clinopyroxene and carbonatite melt under upper mantle conditions. Earth Planet. Sci. Lett. 133, 439–448.
Klimm, K., Blundy, J.D., Green, T.H., 2008. Element partitioning and accessory phase saturation during H2O-saturated melting of basalt with implications for subduction zone chemical fluxes. J. Petrol. 49, 523–553.
Kogarko, L.N., Sorokhtina, N.V., Zaitsev, V.A., Senin, V.G., 2009. Rare metal mineralization of calcite carbonatites from the Cape Verde Archipelago. Geochem. Int. 47, 531–549.
Kulla, G., Hardy, J., 2015. NI 43–101 Blue River Tantalum–Niobium Project, British Columbia, Canada. (Project Update Report).
Leeman, W.P., Tonarini, S., Turner, S., 2017. Boron isotope variations in Tonga-Kermadec-New Zealand arc lavas: Implications for the origin of subduction components and mantle influences. Geochem. Geophy. Geosy. 18, 1126–1162.
Li, H.Y., Li, Y., Ryan, J.G., Li, X., Zhao, R.P., Ma, L., 2019. Molybdenum and boron isotope evidence for fluid-fluxed melting of intraplate upper mantle beneath the eastern North China Craton. Earth Planet. Sci. Lett. 520, 105–114.
Marien, C., Dijkstra, A.H., Wilkins, C., 2018. The hydrothermal alteration of carbonatite in the Fen Complex, Norway: mineralogy, geochemistry, and implications for rare-earth element resource formation. Mineral. Mag. 82, 115–131.
Marschall, H.R., Wanles, V.D., Shimizu, N., Pogge Von Strandmann, P.A.E., Elliott, T., Monteleone, B., 2017. The boron and lithium isotopic composition of mid-ocean ridge basalts and the mantle. Geochim. Cosmochim. Acta 207, 102–138.
Martin, C., Flores, K.E., Harlow, G.E., 2016. Boron isotopic discrimination for subduction-related serpentinites. Geology 44, 899–902.
McDonough, W.F., Sun, S.S., 1995. The composition of the Earth. Chem. Geol. 120, 223–253.
Meert, J.G., Torsvik, T.H., Eide, E.A., Dahlgren, S., 1998. Tectonic significance of the Fen Province, S. Norway: Constraints from geochronology and paleomagnetism. J. Geol. 106, 553–564.
Millonig, L.J., Gerdes, A., Groat, L.A., 2012. U-Th-Pb geochronology of meta-carbonatites and meta-alkaline rocks in the southern Canadian Cordillera: a geodynamic perspective. Lithos 152, 202–217.
Millonig, L.J., Gerdes, A., Groat, L.A., 2013. The effect of amphibolite facies metamorphism on the U-Th-Pb geochronology of accessory minerals from meta-carbonatites and associated meta-alkaline rocks. Chem. Geol. 353, 199–209.
Mitchell, R., Chudy, T., McFarlane, C.R.M., Wu, F.Y., 2017. Trace element and isotopic composition of apatite in carbonatites from the Blue River area (British Columbia, Canada) and mineralogy of associated silicate rocks. Lithos 286-287, 75–91.
Mitchell, R.H., 2005. Carbonatites and carbonatites and carbonatites. Can. Mineral. 43, 2049–2068.
Monger, J., Price, R., 2002. The Canadian Cordillera: geology and tectonic evolution. Canadian Society of Economic Geologists Recorder 17–36.
Mourtada, S., Le Bas, M.J., Pin, C., 1997. Petrogenesis of Mg-carbonatites from Tamazert in the Moroccan High Atlas. C. R. Acad. Sci. Ser. IIA Earth Planet. Sci. 325 (8), 559–564.
Nelson, D.R., Chivas, A.R., Chappell, B.W., McCulloch, M.T., 1988. Geochemical and isotopic systematics in carbonatites and implications for the evolution of ocean-island sources. Geochim. Cosmochim. Acta 52, 1–17.
Pell, J., 1987. Alkaline Ultrabasic Rocks in British Columbia: Carbonatites, Nepheline Syenites, Kimberlites, Ultramafic Lamprophyres and Related Rocks. Ministry of Energy Mines and Petroleum Resources, Province of British Columbia (1987-17, Open File Report).
Pell, J., Höy, T., 1989. Carbonatites in a continental margin environment - the Canadian Cordillera. In: Bell, K. (Ed.), Carbonatites - Genesis and Evolution. Unwin Hyman, London, pp. 200–221.
Pell, J., Simony, P.S., 1987. New correlations of Hadrynian strata, south-central British Columbia. Can. J. Earth Sci. 24, 302–313.
Plank, T., 2005. Constraints from Thorium/Lanthanum on sediment recycling at subduction zones and the evolution of the continents. J. Petrol. 46, 921–944.
Platt, R.G., Woolley, A.R., 1990. The carbonatites and fenites of Chipman Lake. Ontario. Can. Mineral. 28, 241–250.
Rainbird, R.H., Ernst, R.E., 2001. The sedimentary record of mantle plume uplift. In: In: Ernst, R.E., Buchan, K.L. (Eds.), Mantle Plumes: Their Identification through Time, vol. 352. pp. 227–245 Geol. Soc. Spec. Pap.
Read, P.B., Woodsworth, G.J., Greenwood, H.J., Ghent, E.D., Evenchick, C.A., 1991. Metamorphic Map of the Canadian Cordillera, Geological survey of Canada. Map 1714A (scale 1:2 000 000).
Roden, M.F., Murthy, V.R., Gaspar, J.C., 1985. Sr and Nd isotopic compositions of the Jacupiranga carbonatite. J. Geol. 93, 212–220.

Rosatelli, G., Stoppa, F., Jones, A.P., 2000. Intrusive calcio-carbonatite occurrences from Mt. Vulture volcano, southern Italy. Mineral. Mag. 64, 615–624.
Rukhlov, A.S., Chudy, T.C., Arnold, H., Miller, D., 2018a. Field trip guidebook to the Upper Fir carbonatite-hosted Ta-Nb deposit, Blue River area, east-Central British Columbia. British Columbia Ministry of Energy, Mines and Petroleum Resources, British Columbia Geological Survey GeoFile 2018–06.
Rukhlov, A.S., Mao, M., Spence, J., Creaser, R.A., Czech, E., Gabites, J., 2018b. Mineral Chemistry and Isotopic Systematics of Carbonatites and Related Rocks from the Blue River Area. British Columbia Ministry of Energy, Mines and Petroleum Resources, British Columbia Geological Survey GeoFile. (2018–01).
Rukhlov, A.S., Aspler, L.B., Gabites, J., 2019. Cordilleran Carbonatite Hosts of Ta, Nb and REE from the Deep Mantle? British Columbia Ministry of Energy, Mines and Petroleum Resources, British Columbia Geological Survey GeoFile. (2019–08).
Sage, R.P., 1985. Geology of Carbonatite-Alkalic Rock Complexes of Ontario. Chipman Lake Area. Districts of Thunder Bay and Cochrane. Ontario Geological Survey Study 44.
Saunders, A.D., Jones, S.M., Morgan, L.A., Pierce, K.L., Widdowson, M., Xu, Y.G., 2007. Regional uplift associated with continental large igneous provinces: the roles of mantle plumes and the lithosphere. Chem. Geol. 241, 282–318.
Sevigny, J., Simony, P.S., 1989. Geometric relationship between the Scrip Nappe and metamorphic isograds in the northern Adams River are, Monashee Mountains, British Columbia. Can. J. Earth Sci. 26, 606–610.
Sevigny, J.H., Parrish, R.R., Ghent, E.D., 1989. Petrogenesis of Peraluminous Granites, Monashee Mountains, Southeastern Canadian Cordillera. J. Petrol. 30, 557–581.
Simonetti, A., Bell, K., 1993. Isotopic disequilibrium in clinopyroxenes from nephelinitic lavas, Napak volcano, eastern Uganda. Geology 21, 243–246.
Simonetti, A., Bell, K., Viladkar, S.G., 1995. Isotopic data from the Amba Dongar Carbonatite Complex, west-Central India: evidence for an enriched mantle source. Chem. Geol. 122, 185–198.
Simonetti, A., Goldstein, S.L., Schmidberger, S.S., Viladgar, S.G., 1998. Geochemical and Nd, Pb, and Sr Isotope data from deccan alkaline complexes-inferences for mantle sources and plume–lithosphere interaction. J. Petrol. 11–12, 1847–1864.
Sleep, N.H., 1990. Hotspots and mantle plumes: some phenomenology. J. Geophys. Res. 95, 6715–6736.
Spivack, A.J., Edmond, J.M., 1987. Boron isotope exchange between seawater and the oceanic crust. Geochim. Cosmochim. Acta 51, 1033–1043.
Stacey, J.S., Kramers, J.D., 1975. Approximation of Terrestrial Lead Isotope Evolution by a 2-Stage Model. Earth Planet. Sci. Lett. 26, 207–221.
Sweeney, R.J., Prozesky, V., Przybylowicz, W., 1995. Selected trace and minor element partitioning between peridotite minerals and carbonatite melts at 18–46 kb pressure. Geochim. Cosmochim. Acta 59 (18), 3671–3683.
Wallace, M.E., Green, D.H., 1988. An experimental determination of primary carbonatite magma composition. Nature 335, 343–346.
Walowski, K.J., Kirstein, L.A., De Hoog, J.C.M., Elliott, T.R., Savov, I.P., Jones, R.E., EIMF, 2019. Investigating Ocean Island Mantle Source Heterogeneity with Boron Isotopes in Melt Inclusions. pp. 97–108 vol. 508.
Woolley, A.R., 1989. The Spatial and Temporal Distribution of Carbonatites: Carbonatites: Genesis and Evolution. Unwin Hyman, pp. 15–37.
Woolley, A.R., Church, A.A., 2005. Extrusive carbonatites: a brief review. Lithos 85, 1–14.
Woolley, A.R., Kempe, D.R.C., 1989. Carbonatites: Nomenclature, average chemical compositions, and element distribution. In: Bell, K. (Ed.), Carbonatites: Genesis and Evolution. Unwin Hyman, London, pp. 1–13.
Woolley, A.R., Kjarsgaard, B.A., 2008. Carbonatite Occurrences of the World: Map and Database. Geological Survey of Canada (Open File Report 5796).
Worley, B.A., Cooper, A.F., Hall, C.E., 1995. Petrogenesis of carbonate-bearing nepheline syenites and carbonatites from Southern Victoria Land, Antarctica: origin of carbon and the effects of calcite-graphite equilibrium. Lithos 35, 183–199.
Wu, F.Y., Mitchell, R.H., Li, Q.L., Zhang, C., Yang, Y.H., 2016. Emplacement age and isotopic composition of the Prairie Lake carbonatite complex, Northwestern Ontario, Canada. Geol. Mag. 154 (2), 217–236.
Wunder, B., Meixner, A., Romer, R.L., Wirth, R., Heinrich, W., 2005. The geochemical cycle of boron: constraints from boron isotope partitioning experiments between mica and fluid. Lithos 84, 206–216.
Xu, C., Wang, L., Song, W., Wu, M., 2010. Carbonatites in China: a review for genesis and mineralization. Geosci. Front. 1, 105–114.
Ying, Y., Chen, W., Lu, J., Jiang, S.Y., Yang, Y., 2017. In situ U–Th–Pb ages of the Miaoya carbonatite complex in the South Qinling orogenic belt, central China. Lithos 290-291, 159–171.
Zindler, A., Hart, S.R., 1986. Chemical dynamics. Annu. Rev. Earth Pl. Sc. 14, 493–571.

Further Reading

Balboni, E., Jones, N., Spano, T., Simonetti, A., Burns, P.T., 2016. Chemical and Sr isotopic characterization of North America uranium ores: Nuclear forensic applications. Appl. Geochem. 74, 24–32.
Coplen, T.B., Kendall, C., Hopple, J., 1983. Comparison of stable isotope reference samples. Nature 302, 236–238.
Craig, H., 1961. Standard for reporting concentrations of deuterium and oxygen-18 in natural waters. Science 133, 1833–1834.
Jenner, G.A., Longerich, H.P., Jackson, S.E., Fryer, B.J., 1990. ICP-MS-A powerful tool for high-precision trace-element analysis in earth sciences: evidence from analysis of selected U.S.G.S. reference samples. Chem. Geol. 83 (1–2), 133–148.
Koeman, E.C., Simonetti, A., Burns, P.C., 2015. Sourcing of copper and lead within red inclusions from Trinitite post-detonation material. Anal. Chem. 87, 5380–5386.
Manhes, G., Minster, J.F., Allègre, C.J., 1978. Comparative uranium-thorium-lead and rubidium-strontium study of the Saint Sèverin amphoterite: consequences for early solar system chronology. Earth Planet. Sci. Lett. 39 (1), 14–24.
Simonetti, A., Gariépy, C., Banic, C., Tanabe, R., Wong, H.K., 2004. Pb isotopic characterization of aircraft-sampled emissions from the Horne smelter at Noranda (Québec) – implications for atmospheric pollution in northeastern North America. Geochim. Cosmochim. Acta 68, 3285–3294.
Tanaka, T., Togashi, S., Kamioka, H., Amakawa, H., Kagami, H., Hamamotod, T., Yuhara, M., Orihashi, Y., Yoneda, S., Shimizu, H., Kunimaru, T., Takahashi, K., Yanagii, T., Nakano, T., Fujimaki, H., Shinjo, R., Asaharaa, Y., Tanimizu, M., Dragusan, C., 2000. JNdi-1: a neodymium isotopic reference in consistency with LaJolla neodymium. Chem. Geol. 168, 279–281.